

# Excited states in poly-diacetylene chains: A Density-matrix-renormalization-group study

Gergely Barcza<sup>1</sup>, William Barford<sup>2</sup>, Florian Gebhard<sup>3</sup>, and Örs Legeza<sup>1,3</sup>

<sup>1</sup> *Strongly Correlated Systems Lendület Research Group, Wigner Research Centre,  
Hungarian Academy of Sciences, H-1121 Budapest, Hungary*

<sup>2</sup> *Department of Chemistry, University of Oxford, Oxford, OX1 3QZ, United Kingdom*

<sup>3</sup> *Department of Physics and Material Sciences Center, Philipps-Universität D-35032 Marburg, Germany*

(Dated: March 11, 2013)

We study theoretically poly-diacetylene chains diluted in their monomer matrix. We employ the density-matrix renormalization group method (DMRG) on finite chains to calculate the ground state and low-lying excitations of the corresponding Peierls–Hubbard–Ohno Hamiltonian which is characterized by the electron transfer amplitude  $t_0$  between nearest neighbors, by the electron-phonon coupling constant  $\alpha$ , by the Hubbard interaction  $U$ , and by the long-range interaction  $V$ . We treat the lattice relaxation in the adiabatic limit, i.e., we calculate the polaronic lattice distortions for each excited state. Using chains with up to 102 lattice sites, we can safely perform the extrapolation to the thermodynamic limit for the ground-state energy and conformation, the single-particle gap, and the energies of the singlet exciton, the triplet ground state, and the optical excitation of the triplet ground state. The corresponding gaps are known with high precision from experiment. We determine a coherent parameter set ( $t_0^* = 2.4$  eV,  $\alpha^* = 3.4$  eV/Å,  $U^* = 6$  eV,  $V^* = 3$  eV) from a fit of the experimental gap energies to the theoretical values which we obtain for 81 parameter points in the four dimensional search space ( $t_0, \alpha, U, V$ ). We identify dark in-gap states in the singlet and triplet sectors as seen in experiment. Using a fairly stiff spring constant, the length of our unit cell is about one percent larger than its experimental value.

PACS numbers: 71.20.Rv, 71.10.Fd, 78.30.Jw, 78.20.Bh

## I. INTRODUCTION

Poly-diacetylene (PDA) chains dispersed with low concentration in their monomer single-crystal matrix are prototypical quasi one-dimensional materials.<sup>1–3</sup> The structural disorder in the chains and their surrounding matrix is tiny, the electronic excitation energies of the diacetylene monomers are much higher than those of the polymer, and the chains' electronic excitations in the energy range of visible light can be measured with a very high accuracy.<sup>4</sup>

Exciton-polaritons have been generated that have been shown to be coherent over tens of micrometers, i.e., several ten thousand monomer units.<sup>5</sup> This observation was confirmed by weight measurements after dissolving the chains and their monomer matrix.<sup>3</sup> Consequently, the opto-electronic properties of the PDAs result from the electrons' mutual interaction and their interaction with the lattice potential, while the influence of disorder is negligible. This makes these materials the perfect testing-ground for theoretical model studies which describe interacting electrons on perfectly ordered chains.

The typical single-particle gap in PDAs is  $E_{\text{gap}} \gtrsim 2.4$  eV, see Sect. II. Density-functional theory band structure calculations in the local-density approximation for generic PDA geometries estimate the bare band-gap to be  $E_{\text{bare gap}} \approx 1.2$  eV, or less.<sup>6</sup> Results from various methods are compiled in table 1 of Ref. [7]; recent calculations using the Perdew-Burke-Ernzerhof global hybrid density functional and the 6-311G(2d,2p) basis set of atom-centered Gaussian functions (geometries from the

TPSS density functional and the 6-31G(d) basis set)<sup>8</sup> give  $E_{\text{bare gap}} \approx 1.6$  eV.<sup>9</sup> The comparison shows that electronic exchange and correlations account for a substantial fraction of the single-particle gap. In contrast to inorganic semiconductors, the exciton binding energy in PDAs amounts to about 20% of the single-particle gap. Such large binding energies suggest that the electron-electron interaction must be treated accurately for the calculation of the optical properties of the PDAs.

In order to describe the optical excitations in PDAs, two approaches have been taken. The first approach starts from an ab-initio density-functional theory calculation of the bare band structure in local-density approximation (LDA), which is then supplemented by an approximate treatment of the residual electron-electron interaction, e.g., the *GW* approximation for the single-particle bands and the Bethe-Salpeter equation (BSE) for the excitons (LDA+*GW*+BSE).<sup>10,11</sup> Actual calculations for the PDAs often omit the *GW* step (Wannier theory).<sup>12</sup> Within this approach, a number of experimental data can be reproduced, e.g., the  $1^1B_u$  exciton binding energy and its polarizability.

This approach is less successful for the triplet sector.<sup>12</sup> Typically, the energy of the triplet ground state is too high. Recall that, if the electron-electron interaction is absent, the energy of the triplet ground state is identical to the single-particle gap. Starting from a weak-coupling description of the electron-electron interaction on the chains, it is difficult to obtain the experimentally observed energy renormalization by a factor of almost three.<sup>13</sup> Moreover, polaronic effects are not considered in the LDA+BSE approach.

The second approach to a theoretical description of the primary excitations in polymers starts from a many-particle model Hamiltonian that describes only the  $\pi$ -electrons and their mutual interaction. Typically, empirical parameters are used for the tight-binding band structure and for the Pariser-Parr-Pople (PPP) potential.<sup>14</sup> With the help of the density-matrix renormalization-group (DMRG) method,<sup>15</sup> the ground state and elementary excitations for such models can be calculated for large chains with very high accuracy. In this way, the electron-electron interaction is treated without resorting to any approximations.

In a recent study,<sup>16</sup> we used the Hubbard-Ohno potential and the tight-binding parameters of Ref. [17] to calculate the binding energy, polarizability and wave function of the singlet exciton, in good agreement with experiment. However, in our previous study we could not reproduce satisfactorily the energy of the triplet ground state. Moreover, we did not take polaronic effects into account. Here, we shall overcome these shortcomings.

In this work, we perform an extensive DMRG study of the Peierls-Hubbard-Ohno Hamiltonian for the  $\pi$ -electrons on a chain. We start from the tight-binding Peierls description of Race et al.<sup>18</sup> but replace their Ohno potential<sup>19</sup> by the Hubbard-Ohno potential.<sup>16</sup> The essential difference between the two parameterizations of the Pariser-Parr-Pople interaction<sup>14</sup> lies in the treatment of the Coulomb interaction for  $\pi$ -electrons on the carbon atom. The local Hubbard repulsion potential is substantially larger than the corresponding Ohno interaction.<sup>20</sup>

Since we are mostly interested in the polaronic effects, we ignore the energetic effects introduced by the ligands  $R, R'$ . Some preliminary studies show that the energy difference between the singlet and triplet ground states is not influenced by the introduction of a local potential for the carbon atoms which are linked to the side groups. We presume that the dominant influence of the side groups comes from the presence (or absence) of strain in the chains. As can be seen from the data for 3BCMU and 4BCMU, different ligands and the resulting strain results in small energetic differences, of about 0.1 eV for the nBCMU family.

The outline of our work is as follows. In Sect. II, we summarize the experimental observations on the singlet and triplet in-gap states in PDAs. In Sect. III, we define the Peierls-Hubbard-Ohno Hamiltonian and the model parameters which provide the basis of our numerical DMRG study. In Sect. IV, we briefly discuss our numerical approach. In Sect. V, we motivate the parameter regime that we choose for our study. In Sect. VI, we present our results. In Sect. VII, we summarize and conclude. Technical details are deferred to the appendices.

## II. EXPERIMENTAL OBSERVATIONS

We start with an overview of the experimental observations relevant for our study.

### A. Ground-state conformation

First, we collect relevant experimental data on the ground-state properties.

#### 1. Lewis structure

The diacetylene monomer building unit is comprised of four carbon atoms. The four outer electrons of each carbon atom are hybridized. Three of them form localized bonds. There are  $\sigma$ -bonds between neighboring carbon atoms on the chain. Two carbon atoms on the chain share a local  $\pi$ -bond made by two  $p_y$  electrons. The other two carbon atoms share  $\sigma$ -bonds to covalent ligands  $R$  and  $R'$ , which are several Ångström long and differ for various members of the PDA family. In this work, we focus on poly-(Butoxy-Carbonyl-nMethylene-Urethane) (poly-nBCMU) chains with  $n = 3, 4$  where the side groups are given by  $R = R' = (\text{CH}_2)_n - \text{OCONH} - \text{CH}_2 - \text{COO} - (\text{CH}_2)_3\text{CH}_3$ .

The fourth carbon electron is delocalized over the carbon backbone in a molecular  $\pi$ -orbital. Due to the Peierls effect, in the ground state the  $\pi$  electrons dimerize the chain into an alternating sequence of short and long bonds. After dimerization, the four carbon atoms in the unit cell are linked by a triple bond, a single bond, a double bond, and a single bond. The corresponding Lewis structure of the ground state is shown in Fig. 1.

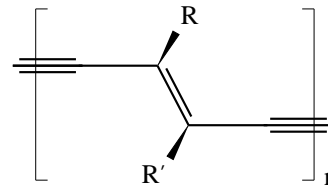


FIG. 1. Lewis structure of a poly-diacetylene unit cell.

#### 2. Lattice parameters

For a high-quality single crystal of Poly-[1,2-bis-(p-tolylsulfonyloxymethylen)-1-buten-3-inylen] (PTS), the atomic distances at room temperature have been measured<sup>21</sup> as  $r_t = 1.191(4)$  Å,  $r_d = 1.356(4)$  Å, and  $r_s = 1.428(4)$  Å [uncertainties in the last digit in brackets] for the triple (t), double (d), and single (s) bonds, respectively. Typical atomic distances for other PDA polymer single crystals are<sup>22</sup>  $r_t = 1.20$  Å,  $r_d = 1.36$  Å, and  $r_s = 1.43$  Å. The same set of data applies for 3BCMU-PDA at low temperatures.<sup>23</sup> The chain of atoms is not straight; the single and double bonds alternately form angles of  $\varphi_1 = 120^\circ$  and  $\varphi_2 = 240^\circ$  degrees, with a temperature variation of a few degrees.<sup>23</sup> In the comparison with our calculations we shall assume that the bond lengths and angles given above for the PDA single crystals are

representative for chains in their diacetylene monomer matrix.

We shall only deal with planar ('blue') PDA chains.<sup>3</sup> The individual polymer chains of 4BCMU are strained in their monomer single crystals but are essentially unstrained in 3BCMU.<sup>23</sup> Strain should be the primary source for differences in the spectra of these two PDAs.

## B. Excited states

Next, we summarize experimental results on the low-lying electronic excitations. PDAs are center-symmetric insulators. Their ground state  $G$  is a spin singlet with symmetry  $A_g$  under inversion.

### 1. Single-particle gap and excited singlet states

The charge gap for single-particle excitations, as determined from Franz-Keldysh oscillations in electro-absorption experiments,<sup>24</sup> is  $E_{\text{gap}}(3\text{BCMU}) = 2.482\text{ eV}$  and  $E_{\text{gap}}(4\text{BCMU}) = 2.378\text{ eV}$  in 3BCMU and 4BCMU chains, respectively.

The excitation energy of the primary singlet exciton  $S$  (symmetry  ${}^1B_u$ ) defines the optical gap,  $\Delta_{\text{opt}}^s = E_S - E_G$ , which amounts to  $\Delta_{\text{opt}}^s(3\text{BCMU}) = 1.896\text{ eV}$  and  $\Delta_{\text{opt}}^s(4\text{BCMU}) = 1.810\text{ eV}$  in 3BCMU and 4BCMU, respectively. Therefore, the singlet exciton binding energy, defined by  $\Delta_{\text{ex}}^s = E_{\text{gap}} - E_S$ , becomes  $\Delta_{\text{ex}}^s(3\text{BCMU}) = 0.586\text{ eV}$  in 3BCMU, and  $\Delta_{\text{ex}}^s(4\text{BCMU}) = 0.568\text{ eV}$  in 4BCMU, about 24% of the band-gap. The energy levels are sketched in Fig. 2.

The singlet exciton is the energetically lowest state in the spin-singlet sector which can be generated by a single-photon absorption process. In addition, there are further, optically dark states in the gap. The existence of optically dark states  $X_1$  and  $X_2$  below the optical gap can be inferred from non-radiative decay processes which are monitored via pump-probe spectroscopy, see Ref. [3] for a review. The exciton rapidly populates the states  $X_{1,2}$  so that they should have the same spin quantum number.

In principle, the energy of singlet states in the gap with  ${}^1A_g$ -symmetry can be determined via two-photon absorption. Two-photon absorption for a single-crystal of the poly-diacetylene paratoluene-sulfonate reveals three gap states with energies  $E_{X_3} = 1.05\Delta_{\text{opt}}^s$ ,  $E_{X_2} = 0.9\Delta_{\text{opt}}^s$ , and  $E_{X_1} = 0.8\Delta_{\text{opt}}^s$ . These states should exist in all PDAs. Note that in the experimental literature,<sup>3</sup> the numbering of the states  $X_1$  and  $X_2$  is reversed.

### 2. Phonon energies

Raman scattering reveals vibrational energies which are assigned to the oscillations of the double (D) and triple (T) bonds. For 3BCMU chains in their monomer matrix they are  $\hbar\omega_D = 0.181\text{ eV}$  and  $\hbar\omega_T = 0.261\text{ eV}$ .<sup>23</sup>

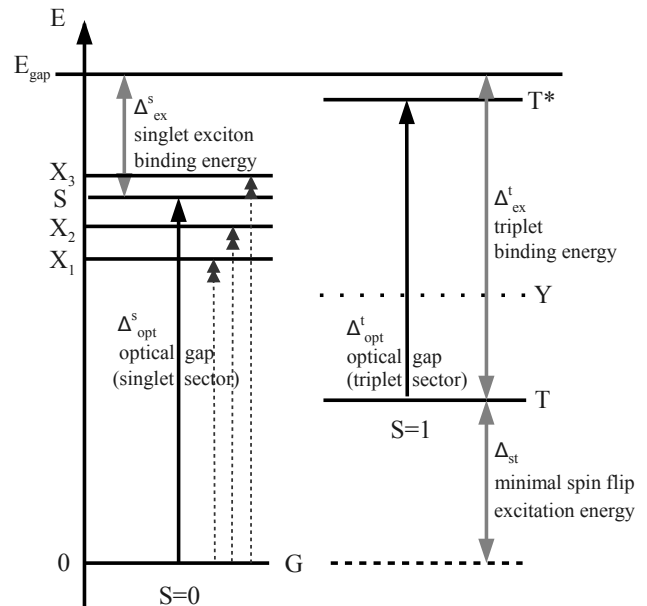


FIG. 2. Energy levels of in-gap states in the spin-singlet and spin-triplet sectors. Single-tip arrows: optical absorption spectroscopy; double-tip arrows: two-photon absorption spectroscopy. Double arrows: binding energies (gaps).  $G$ : singlet ground state ( $1^1A_g$ );  $S$ : singlet exciton ( $1^1B_u$ );  $X_1$ ,  $X_2$ ,  $X_3$ : singlet dark states ( $m^1A_g$ );  $T$ : triplet ground state ( $1^3B_u$ );  $T^*$ : optical excitation of the triplet ground state ( $1^3A_g$ );  $Y$ : dark triplet state ( $m^3B_u$ ).

In accordance with the Raman data, the optical spectra of 3BCMU chains show strong exciton replicas at the energies  $E_c = E_S + \hbar\omega_D = 2.079\text{ eV}$  and at  $E_d = E_S + \hbar\omega_T = 2.160\text{ eV}$ , respectively, when the exciton is accompanied by single optical phonons corresponding to the vibrations with frequencies  $\omega_D$  and  $\omega_T$ .

Electro-absorption measurements<sup>3,25</sup> show that there are more significant single-phonon replicas of the singlet exciton at the energies  $E_{a,b} = E_S + \hbar\omega_{S,D^*}$  with  $\hbar\omega_S = 0.090\text{ eV}$  and  $\hbar\omega_{D^*} = 0.155\text{ eV}$ . Due to the fact that  $E_b \approx E_c$ , the phonon replica at  $E_b$  appears in the low-energy flank of the replica at energy  $E_c$ . The electro-absorption measurements also permit the identification of multi-phonon replicas, e.g., at replica energies  $\hbar(\omega_{D^*} + \omega_D)$ ,  $2\hbar\omega_D$ ,  $\hbar(\omega_D + \omega_T)$ ,  $2\hbar\omega_T$ .<sup>25</sup>

### 3. Triplet ground state and excited triplet states

The triplet sector is more difficult to access experimentally because a transition between the spin-zero ground state  $G$  and the lowest spin-one state  $T$  is optically forbidden. Optical pump-probe spectroscopy<sup>3</sup> reveals that a small fraction of singlet excitons decays into a long-lived state which can be optically excited by the probe pulse. Its long life-time indicates that this in-gap state is the spin-triplet ground state  $T$ . The probe pulse gen-

erates transitions from T to T\* in the triplet sector. The optical gap in the triplet sector is defined as  $\Delta_{\text{opt}}^t = E_{T^*} - E_T$ , and amounts to  $\Delta_{\text{opt}}^t(3\text{BCMU}) = 1.360\text{ eV}$  and  $\Delta_{\text{opt}}^t(4\text{BCMU}) = 1.345\text{ eV}$ , respectively.

Optical pumping above a threshold  $E_f \approx 2.0\text{ eV}$  very efficiently generates states which show a strong optical absorption with energy  $\Delta_{\text{opt}}^t$ . This can be readily understood if the spin-singlet excitations above  $E_f$  fission into triplet pairs.<sup>3</sup> In turn, these triplet pairs can recombine into singlets and decay optically. If we ignore lattice effects (bi-polaron formation), we obtain a reasonable estimate for the energy of the triplet state T,  $\Delta_{\text{st}} = E_T - E_G \approx E_f/2$ . For 3BCMU and 4BCMU this estimate gives  $\Delta_{\text{st}}(3\text{BCMU}) \gtrsim 1.0 \pm 0.05\text{ eV}$  and  $\Delta_{\text{st}}(4\text{BCMU}) \gtrsim 0.95 \pm 0.05\text{ eV}$ , respectively.

The binding energy of the triplet ground state is defined by  $\Delta_{\text{ex}}^t = E_{\text{gap}} - E_T$ . It amounts to  $\Delta_{\text{ex}}^t(3\text{BCMU}) \approx 1.5\text{ eV}$  and  $\Delta_{\text{ex}}^t(4\text{BCMU}) \approx 1.4\text{ eV}$  in 3BCMU and 4BCMU, respectively, more than 60% of the single-particle gap. The energy of the optically excited triplet ground state T\* is found to be  $E_{T^*}(3\text{BCMU}) - E_G = 2.36\text{ eV}$  and  $E_{T^*}(4\text{BCMU}) - E_G = 2.30\text{ eV}$  above the ground state, about 0.1 eV below the threshold  $E_{\text{gap}}$  for single-particle excitations.

The optically dark singlet states X<sub>1</sub> and X<sub>2</sub> decay non-radiatively into a state Y. Its weak population and long life-time indicate that it is reached via intersystem crossing so that it ought to be a spin-triplet state which lies energetically above the triplet ground state T. It should be of symmetry  ${}^3B_u$  so that it cannot be reached via an optical excitation of the triplet ground state.

Fig. 2 shows the experimentally observed level spectrum for PDA chains in the singlet and triplet sectors. We summarize the corresponding values for the in-gap states in table I, and compare them to our theoretical results for our best parameter set, ( $t_0^* = 2.4\text{ eV}$ ,  $\alpha^* = 3.4\text{ eV}/\text{\AA}$ ,  $U^* = 6\text{ eV}$ ,  $V^* = 3\text{ eV}$ ), see Sect. VI.

### III. MODEL DESCRIPTION OF POLY-DIACETYLENE CHAINS

In this work we restrict ourselves to the description of the  $\pi$  electrons because they dominate the optical response of the poly-diacetylene chains immersed in their monomer matrix for energies  $\hbar\omega < 3\text{ eV}$ . In order to make contact with previous work,<sup>18</sup> we treat the other electrons as inert, i.e., they are supposed to form the *unrelaxed* geometry of the carbon backbone. The distance between two carbon atoms is  $R_2$  for a single  $\sigma$ -bond, and  $R_1 < R_2$  for the  $\sigma$ - $p_y$  double bond (extrinsic distortion).

#### A. Electronic Hamiltonian

The motion of  $\pi$ -electrons between neighboring carbon atoms and their mutual Coulomb interactions defines the

Energy	3BCMU	4BCMU	Theory
$E_{X_1}$	1.5	1.4	1.74 [1.94]
$E_{X_2}$	1.7	1.6	1.85 [1.94] <sup>a</sup>
$E_S = \Delta_{\text{opt}}^s$	<b>1.896</b>	<b>1.810</b>	2.00 [2.05]
$E_{X_3}$	2.0	1.9	
$E_{\text{gap}}$	<b>2.482</b>	<b>2.378</b>	2.45 [2.47]
$\Delta_{\text{ex}}^s = E_{\text{gap}} - E_S$	<b>0.586</b>	<b>0.568</b>	0.45 [0.42]
$E_T = \Delta_{\text{st}}$	1.0 $\pm$ 0.05	0.95 $\pm$ 0.05	1.00 [1.06]
$E_{T^*} = \Delta_{\text{st}} + \Delta_{\text{opt}}^t$	2.36 $\pm$ 0.05	2.30 $\pm$ 0.05	2.25
$\Delta_{\text{opt}}^t$	<b>1.360</b>	<b>1.345</b>	1.25 [1.28]
$\Delta_{\text{ex}}^t = E_{\text{gap}} - E_T$	1.5 $\pm$ 0.05	1.4 $\pm$ 0.05	1.45 [1.40]

<sup>a</sup> Several degenerate states are found in DMRG.

TABLE I. First and second column: Excitation energies in 3BCMU and 4BCMU at low temperatures. All energies are measured in eV relative to the energy of the ground state,  $E_G = 0$ . Bold number: directly measured; italic number: estimate. Third column: our results, see Sect. VI; the numbers in square brackets give the excitation energy for the rigid-lattice transition from G ( $E_{\text{gap}}$ ,  $E_S$ ,  $E_{X_{1,2}}$ ,  $E_T$ ) and from T ( $\Delta_{\text{opt}}^t$ ).

electronic problem,

$$\hat{H}_e = \hat{T} + \hat{V}, \quad (1)$$

where  $\hat{T}$  and  $\hat{V}$  specify the electrons' kinetic energy and their mutual interaction, respectively.

#### 1. Kinetic energy

The motion of the  $\pi$ -electrons over the unrelaxed backbone is described by the operator for the kinetic energy,

$$\hat{T} = - \sum_{l;\sigma} t_l \left( \hat{c}_{l,\sigma}^+ \hat{c}_{l+1,\sigma} + \hat{c}_{l+1,\sigma}^+ \hat{c}_{l,\sigma} \right), \quad (2)$$

where  $\hat{c}_{l,\sigma}^+$ ,  $\hat{c}_{l,\sigma}$  are creation and annihilation operators, respectively, for a  $\pi$ -electron with spin  $\sigma = \uparrow, \downarrow$  on site  $l$  with two-dimensional coordinate  $\vec{r}_l = (x_l, y_l)^T$ . The matrix elements  $t_l$  are the electron transfer amplitudes between neighboring sites. Transfer amplitudes between next-nearest neighbors should be included to fit better the band structure of all carbon electrons.<sup>9</sup> The amplitude for an electron transfer between two carbon sites at distance  $r_0 = 1.4\text{ \AA}$  is given by  $t_0$  which we use as an adjustable parameter.

We consider the half-filled band exclusively, i.e., in the ground state and for the excitations in Fig. 2 the number of  $\pi$  electrons  $N_e$  equals the number of lattice sites  $N$ .

#### 2. Coulomb interaction

The diacetylene monomer single-crystals are insulators, and also the PDA chains display a finite charge gap.

Therefore, the long-range Coulomb interaction is not dynamically screened at the energy scale of a few electron volts.

Therefore, we start from the Pariser-Parr-Pople (PPP) interaction<sup>14</sup>

$$\hat{V} = U \sum_{l=1}^N \left( \hat{n}_{l,\uparrow} - \frac{1}{2} \right) \left( \hat{n}_{l,\downarrow} - \frac{1}{2} \right) + \frac{1}{2} \sum_{l \neq m=1}^N V_{l,m}^{\text{PPP}} [(\hat{n}_l - 1)(\hat{n}_m - 1)] . \quad (3)$$

Here,  $\hat{n}_l = \hat{n}_{l,\uparrow} + \hat{n}_{l,\downarrow}$  counts the number of electrons on site  $l$ , and  $\hat{n}_{l,\sigma} = \hat{c}_{l,\sigma}^\dagger \hat{c}_{l,\sigma}$  is the local density operator at site  $l$  for spin  $\sigma$ . The strength of the (local) Hubbard interaction is parameterized by  $U$ , and  $V_{l,m}$  are the PPP parameters for the effective Coulomb repulsion between electrons at different positions  $\vec{r}_l$  and  $\vec{r}_m$ .

For the description of electrons and holes in quantum wires and other quasi one-dimensional structures in vacuum, various effective potentials have been used in the literature.<sup>26,27</sup> For example, in our previous study<sup>16</sup> we used the erf-potential ( $x = |\vec{r}_l - \vec{r}_m|$ )

$$V_{l,m}^{\text{erf}} = V^{\text{erf}}(x) = \frac{e^2}{\epsilon_d R} \sqrt{\pi} \exp[(x/R)^2] [1 - \text{erf}(x/R)] , \quad (4)$$

where  $\text{erf}(x)$  is the error function,  $R$  is the adjustable confinement parameter, and  $\epsilon_d = 2.3$  is the static dielectric constant for the diacetylene monomer matrix. In general, the PPP interaction for the  $\pi$ -electrons on the chain in the surrounding matrix has the form

$$V_{l,m}^{\text{PPP}} = V^{\text{PPP}}(x) = V^{\text{erf}}(x) \frac{\epsilon_d}{\epsilon(x)} , \quad (5)$$

where  $\epsilon(x)$  is the static dielectric function at distance  $x = |\vec{r}_l - \vec{r}_m|$  with  $\epsilon(x \rightarrow \infty) = \epsilon_d$ . Unfortunately, the short-distance behavior of  $\epsilon(x)$  is unknown.

In this work we follow Refs. [16, 17, and 20] and approximate the Pariser-Parr-Pople interaction using the Hubbard-Ohno potential, i.e., for  $x = |\vec{r}_l - \vec{r}_m| \neq 0$  we set

$$V_{l,m}^{\text{PPP}} \approx V_{l,m}^{\text{Ohno}} = V^{\text{Ohno}}(x) = \frac{V}{\epsilon_d \sqrt{1 + \beta(x/\text{\AA})^2}} , \quad (6)$$

$$\beta = \left( \frac{V}{14.397 \text{ eV}} \right)^2 .$$

The Ohno potential and its adjustable parameter  $V$  describe the effective strength of the Coulomb interaction at short distances; for large electron-electron distances,  $V^{\text{Ohno}}(x \rightarrow \infty) \rightarrow e^2/(\epsilon_d x)$  because  $e^2 = 14.397 \text{ eV \AA}$ . Note that  $U$  and  $V$  are independent adjustable parameters in our theory. Later, we shall assume that the screening of the on-site interaction is substantially less effective than for the long-range interaction.

The eigenstates of the electronic problem follow from the solution of the corresponding Schrödinger equation,

$$\hat{H}_e |\Psi\rangle = E_\Psi |\Psi\rangle . \quad (7)$$

We denote expectation values of operators  $\hat{A}$  in the normalized state  $|\Psi\rangle$  as  $\langle \hat{A} \rangle = \langle \Psi | \hat{A} | \Psi \rangle$ .

### 3. Particle-hole symmetry

The Hamiltonian (8) is invariant under the particle-hole transformation  $\hat{c}_{l,\sigma} \mapsto (-1)^l \hat{c}_{l,-\sigma}^\dagger$ . At half band-filling, the ground state  $|\text{G}\rangle$  is also invariant under this transformation.

In our numerical investigation, we calculate important excited states using the proper quantum numbers for the spin symmetry ( $S = 0, 1$ ;  $p = 2S + 1$ ), inversion symmetry ( $X = A_g, B_u$ ), and particle-hole symmetry ( $v = \pm 1$ ). Therefore, we label states in the form  $m \ ^p X^v$  where  $m \geq 1$  counts the states with the same symmetry in ascending energetic order. The quantum numbers for the most prominent in-gap states are summarized in table II.

	State			
Symmetry	G	T	S	T*
Spin ( $S$ )	0	1	0	1
Inversion ( $X$ )	1	-1	-1	1
Particle-hole ( $v$ )	1	1	-1	-1
Classification	1 $^1 A_g^+$	1 $^3 B_u^+$	1 $^1 B_u^-$	1 $^3 A_g^-$

TABLE II. Quantum numbers of important in-gap states. For the definition of the states, see Fig. 2.

### B. Electron-lattice interaction

The electron-phonon coupling leads to the dimerization of the ground-state structure (Peierls effect). Moreover, excitations carry a polaron cloud, and the polaronic shifts in the single-particle excitation energies will in general be different from those of bound pairs. For example, the singlet exciton fissions into a bound pair of triplet polarons. This bipolaron has an energy which is lower than twice the energy of a triplet polaron. Therefore, the estimates in table I provide lower bounds for  $\Delta_{\text{st}}$ .

Due to the (small) Peierls distortion, the energy increases so that the total Hamiltonian reads

$$\hat{H} = \hat{H}_e + \sum_{l=1}^{N-1} \frac{\delta_l^2}{4\pi t_0 \lambda_l} . \quad (8)$$

At distance  $r_0 = 1.4 \text{ \AA}$ , the electron transfer matrix element is given by our adjustable parameter  $t_0$ . The strength of the electron-lattice coupling is parameterized by the coupling constant<sup>28,29</sup>

$$\lambda_l = \frac{2\alpha^2}{\pi K_l t_0} \quad (9)$$

where  $\alpha$  is the strength of the Peierls coupling and  $K_l$  are the elastic constants for the carbon backbone, namely,

$K$  for the  $\sigma$ -bonds and  $G > K$  for the  $\sigma$ - $p_y$  bonds,  $K_l = K + \delta_{l \bmod 4, 1}(G - K)$ . The parameters  $\alpha$ ,  $K$ , and  $G$  must be adjusted. In effect, we address the region where  $\lambda_l < 0.1$  so that the adiabatic approximation is valid, i.e., we may treat the lattice distortions classically.

The intrinsic Peierls distortion implies a modulation of the bond lengths,

$$\delta r_l = r_l - R_l = -\frac{\delta_l}{2\alpha}. \quad (10)$$

Here,  $R_2 = r_0$  for a single  $\sigma$ -bond of the carbon backbone chain and  $R_1 = r_0 - \delta^e/(2\alpha)$  for its  $\sigma$ - $p_y$  double bond. The size of the extrinsic dimerization  $\delta^e$  is calculated in App. A. As a result of the intrinsic Peierls dimerization, the ground-state unit cell of the distorted chain consists of four carbon atoms, linked by a single bond, a double bond, a single bond, and a triple bond, see Fig. 1.

The energies  $\delta_l$  modulate the electron transfer amplitudes,

$$t_l = \bar{t}_l + \delta_l/2 \quad (11)$$

with

$$\bar{t}_l = t_0 + \delta^e/2 \quad (\text{undistorted } \sigma\text{-}p_y \text{ double bond}), \quad (12)$$

$$\bar{t}_l = t_0 \quad (\text{undistorted } \sigma \text{ single bond}). \quad (13)$$

Note that, for small distortions, the transfer matrix elements for the single, double, and triple bonds in the ground state obey

$$t_{s,d,t} = t_0 - \alpha(r_{s,d,t} - r_0), \quad (14)$$

where  $r_s$ ,  $r_d$ , and  $r_t$  are the lengths of the single, double, and triple bond in the unit cell, see eq. (10).

### C. Model parameters

Our model employs the following parameters: (i) The electron transfer matrix element  $t_0$  for a single C–C bond at distance  $r_0 = 1.4 \text{ \AA}$ ; (ii) the strength of the local Hubbard interaction  $U$ ; (iii) the strength of the short-range Coulomb interaction  $V$ ; (iv) the Peierls coupling  $\alpha$ ; (v) the spring constants  $K$  and  $G$ . The model parameters are adjusted to reproduce the single-particle gap  $E_{\text{gap}}$ , the singlet exciton energy  $E_S$ , the energy of the triplet state  $E_T$ , and the optical gap in the triplet sector  $\Delta_{\text{opt}}^t$ , see table I. Moreover, we estimate the values for the spring constants from the energy of the phonon replicas.

Of course, we cannot scan a five-dimensional parameter space completely. Therefore, we have to restrict ourselves to values which seem plausible, see Sect. V. The model parameters investigated are summarized in table III.

Fixed parameter	Value	Control parameter	Range of values
$\epsilon_d$	2.3	$t_0$	2.0 eV ... 2.4 eV
$K$	44 eV/ $\text{\AA}^2$	$V$	2 eV ... 3 eV
$G$	68 eV/ $\text{\AA}^2$	$U$	5 ... 6 eV
$r_0$	1.4 $\text{\AA}$	$\alpha$	3.4 eV/ $\text{\AA}$ ... 3.6 eV/ $\text{\AA}$

TABLE III. Parameters of the Peierls–Hubbard–Ohno model.

## IV. METHOD

First, we outline our procedure to find the optimal lattice structure. Next, we define the single-particle gap and describe how we address excited in-gap states. Lastly, we remark on our DMRG procedure and the extrapolation of our finite-size data to the thermodynamic limit.

In this section and in the remainder of the paper, all energies ( $t_0, U, V; E_{\text{gap}}, \Delta_{\text{opt}}^s, \Delta_{\text{st}}, \Delta_{\text{opt}}^t$ ) are given in eV, all lengths are given in  $\text{\AA}$ , and  $\alpha$  is given in units of eV/ $\text{\AA}$ .

### A. Optimization of the lattice structure

#### 1. Procedure

The values for the electron transfer amplitude modulations follow from minimization of the energy functional  $E_\Psi(\delta_l) = \langle \Psi | \hat{H} | \Psi \rangle$  for the normalized state  $|\Psi\rangle$  which can be the ground state or any excited state of  $\hat{H}$ . The actual values for the dimerization are obtained from the minimization of the energy functional  $E_\Psi(\delta_l)$  with respect to  $\delta_l$  subject to the constraint

$$\sum_{l=1}^{N-1} \delta_l = 0. \quad (15)$$

This reflects the fact that the total chain length should be fixed; see below. The condition (15) is taken into account with the help of the Lagrange multiplier  $\Gamma$ .

According to the Hellmann–Feynman theorem,<sup>30</sup> the negative derivatives of the energy functional with respect to  $\delta r_l$  define the force fields  $f_l$ ,

$$-\frac{f_l}{2\alpha} = -\frac{\delta_l}{2\pi t_0 \lambda_l} - \Gamma + F_l[\delta_p], \quad (16)$$

$$\begin{aligned} F_l[\delta_p] = & \frac{1}{2} \left\langle \sum_{\sigma} \left( \hat{c}_{l,\sigma}^+ \hat{c}_{l+1,\sigma} + \hat{c}_{l+1,\sigma}^+ \hat{c}_{l,\sigma} \right) \right\rangle \\ & + \frac{1}{2\epsilon_d} \sum_{i \neq j=1}^N \frac{\beta V / \text{\AA}^2}{[1 + \beta(|\vec{r}_i - \vec{r}_j| / \text{\AA})^2]^{3/2}} \\ & \times \left[ x_{i,j} \frac{\partial x_{i,j}}{\partial \delta_l} + y_{i,j} \frac{\partial y_{i,j}}{\partial \delta_l} \right] \langle (\hat{n}_i - 1)(\hat{n}_j - 1) \rangle, \end{aligned} \quad (17)$$

where  $\delta_p$  ( $p = 1, \dots, N-1$ ) are the Peierls modulations of the electron transfer amplitudes and  $x_{i,j} = x_i - x_j$ ,  $y_{i,j} = y_i - y_j$ .

For fixed bond angles,  $x_l$  and  $y_l$  are defined as  $x_l = x_{l-1} + r_l \cos(60^\circ)$  and  $y_l = y_{l-1} - r_l \sin(60^\circ)$  for the bonds at an angle of  $120^\circ$ , and  $x_l = x_{l-1} + r_l$  and  $y_l = y_{l-1}$  otherwise, with  $r_l = R_l - \delta_l/(2\alpha)$  from (10). The force fields  $f_l$  are zero at the optimal values  $\delta_l^{\text{opt}}$  for a chosen state  $|\Psi\rangle$ . Note that  $|\Psi\rangle$  is an eigenstate of the electronic problem which is parameterized in terms of  $\delta_p$ . Therefore, the minimization of the force fields has to be done self-consistently.<sup>18</sup>

- i. In step  $k$  of the iteration ( $k = 1, 2, \dots$ ), the target eigenstate  $|\Psi_k\rangle$ , e.g.,  $G_k$ ,  $S_k$ , or  $T_k$ , is calculated for  $\delta_{k;l}$  using the infinite-lattice DMRG algorithm. In all our cases, the initial choice  $\delta_{1;l} = 0$  for  $l = 1, \dots, N-1$  leads to converged solutions.

- ii. For given  $k$  and fixed quantum-mechanical expectation values in  $|\Psi_k\rangle$ , the distortion energies are determined iteratively.

To this end, the condition  $f_l = 0$  in (16) is used to determine the distortion energies for the next iteration,  $\delta_{k;l}^{n+1} = 2\pi t_0 \lambda_l (-\Gamma_k^n + F_l[\delta_{k;p}^n])$ , ( $n \geq 0$ ,  $\delta_{k;l}^0 = \delta_{k;l}$ ). Here, the Lagrange parameter follows from (15) as  $\Gamma_k^n = \sum_l \lambda_l F_l[\delta_{k;p}^n] / \sum_l \lambda_l$ .

The distortion energies typically converge after some five to fifteen iterations. The converged solution defines  $\delta_{k+1;l} = \lim_{n \rightarrow \infty} \delta_{k;l}^n$  for the next iteration in  $k$ .

- iii. The steps (i) and (ii) are repeated until a converged set of distortion energies and DMRG energies for the states are obtained,  $\delta_l = \lim_{k \rightarrow \infty} \delta_{k;l}$ ,  $|\Psi\rangle = \lim_{k \rightarrow \infty} |\Psi_k\rangle$ .

Strictly speaking, the condition of a fixed chain length  $\ell_c$  corresponds to  $x_{1,N}^2 + y_{1,N}^2 = \ell_c^2$ . We have verified numerically that the condition (15) preserves the chain length up to 0.1% for  $N \lesssim 100$ .

## 2. Polaronic energies

It is important to note that we optimize the lattice structure and the corresponding distortion energies for each state separately. Our excited states contain all polaronic energy contributions, i.e., we give their *relaxed* energies. This polaronic relaxation was not taken into account in our previous study.<sup>16</sup> There, we studied *rigid-lattice* transitions with fixed electron transfer amplitudes  $t_s$ ,  $t_d$ , and  $t_t$ , which correspond to the Lewis structure of Fig. 1. In general, they are higher in energy than the corresponding *relaxed* excitations.

It is not a priori clear whether the relaxed or the rigid-lattice energies should be compared to experiment. For the optical singlet excitation, no Stokes shift is observed between absorption and fluorescence spectra<sup>3</sup> so that, in the Franck-Condon picture, the exciton creation process corresponds to a vertical transition.

In order to estimate the polaronic contribution to the energy, we calculate the energy of excited states in the rigid-lattice approximation for our optimal parameter set, see Sect. VI. For ( $t_0^* = 2.4$  eV,  $\alpha^* = 3.4$  eV/Å,  $U^* = 6$  eV,  $V^* = 3$  eV), the relaxed energy of the single-particle gap is  $E_{\text{gap}}^{\text{relaxed}} = 2.45$  eV whereas the energy of a single-particle excitation with fixed electron transfer matrix elements  $t_s^G$ ,  $t_d^G$ , and  $t_t^G$  leads to  $E_{\text{gap}}^{\text{rigid}} = 2.47$  eV, see table I. Thus, the energy relaxation due to the polaron formation amounts to about  $\delta_{\text{polaron}} = 0.02$  eV. In the band picture, the singlet exciton is a bound state of particle-hole excitations. Correspondingly, the polaronic shift in  $E_S$  should be about twice as large as  $\delta_{\text{polaron}}$ , as indeed observed,  $E_S^{\text{relaxed}} = 2.00$  eV and  $E_S^{\text{rigid}} = 2.05$  eV, so that  $E_S^{\text{rigid}} - E_S^{\text{relaxed}} = 0.05$  eV  $\approx 2\delta_{\text{polaron}}$ .

The same amount of polaronic relaxation energy is observed for the singlet-triplet gap,  $E_T^{\text{rigid}} - E_T^{\text{relaxed}} = 0.06$  eV. When we start from the relaxed triplet ground state, we find for the optically excited state  $T^*$  that  $E_{T^*}^{\text{rigid}} = 1.28$  eV whereas  $E_{T^*}^{\text{relaxed}} = 1.25$  eV. It is seen that the polaronic relaxation energy amounts to about  $\delta_{\text{polaron}}$  also in the triplet sector.

Our observation of a fairly small polaronic relaxation energy ties in with the fact that our electron-lattice coupling is small,  $\lambda_l < 0.1$ , and the adiabatic approximation is valid. In our comparison with experiment below, we show the energies for transitions between lattice-relaxed configurations.

## B. Single-particle gap and in-gap excitations

The band-gap or single-particle gap  $E_{\text{gap}}$  is defined by the difference in chemical potentials for a system with  $N_e$  and  $N_e - 1$  particles,

$$\begin{aligned} E_{\text{gap}} &= \mu(N_e) - \mu(N_e - 1), \\ \mu(N_e) &= E_G(N_e + 1) - E_G(N_e), \end{aligned} \quad (18)$$

where  $E_G(N_e)$  is the energy of the  $N_e$ -particle ground state G. In the presence of particle-hole symmetry at half band-filling, we have

$$E_{\text{gap}} = 2\mu(N_e) \quad (19)$$

for the minimal energy of a single-particle excitation.

In poly-diacetylenes, the singlet exciton and its vibronic replicas carry most of the oscillator strength of the optical excitations. The quadratic Stark effect in the electro-absorption proves that they are bound states of electron-hole excitations.<sup>31</sup> The exciton energy thus defines the optical gap,

$$\Delta_{\text{opt}}^s = E_S(N_e = N) - E_G(N_e = N), \quad (20)$$

where  $E_S(N_e = N)$  is the energy of the first excited state of the half-filled system with symmetry  $B_u$ . The binding energy of the exciton is then obtained as

$$\Delta_{\text{ex}}^s = E_{\text{gap}} - E_S. \quad (21)$$

Note that we calculate for finite-size systems so that all quantities must be extrapolated into the thermodynamic limit,  $N \rightarrow \infty$ .

For a full account of all in-gap states, we target up to five states simultaneously in the spin-singlet and spin-triplet sectors, respectively. Note that the lattice relaxation must be done for each state separately. These calculations represent the most time consuming part of our investigations.

### C. Numerical procedure

In this work we present results from numerical density-matrix renormalization-group (DMRG)<sup>15</sup> calculations on finite chains with open boundary condition (OBC) using an adopted version used previously.<sup>16</sup> The discarded weight was kept below  $\eta = 10^{-6}$  for all calculations by employing the dynamical block-state selection (DBSS) procedure.<sup>32,33</sup> We have set the minimum number of block states to  $M_{\min} = 400$  and used three sweeps. The maximum value of the number of block states varied around  $M_{\max} = 600$ . As benchmarks we compared our DMRG energies for some selected parameter values with those from a DMRG code used earlier by Race, Barford, and Bursill.<sup>18</sup> The latter one, however, only uses the infinite-lattice procedure so that our variational energies are always slightly lower.

The ground state as well as all excited states have been targeted and relaxed individually using  $k = 5$  to 15 relaxation iteration steps to reach the pre-set convergence criterion on  $\delta_l$ . Note that each relaxation iteration step requires a full DMRG run with three sweeps. The whole relaxation procedure has been performed for all target states and for all chain lengths independently from  $N = 6$  up to  $N = 66$ , in steps of  $\Delta N = 4$ . For our optimized parameter set we have performed calculations for up to  $N = 102$  sites.

The spin multiplicity of the converged target states was calculated from the expectation value of the operator for the total spin  $\hat{S}^2$ , employing the expectation values of the corresponding correlation functions.<sup>34</sup> In order to determine the optically dark in-gap singlet states we have shifted the energies of the triplet states out of the gap by adding the term  $\sum_{ij} S_i^- S_j^+$  to the Hamiltonian. As an alternative procedure, we have also identified the exciton states by calculating the dipole strength as introduced in Ref. [16] in which the reduced density matrix of the target state was constructed from the reduced density matrices of the ten lowest eigenstates.

For the 81 parameter points of the four-dimensional search space  $(t_0, \alpha, U, V)$  and for the energies of the states  $(G, S, E_{\text{gap}}, T, T^*, X_l, Y_l)$  shown in Fig. 2, we have taken on average  $k = 10$  relaxation steps for the 16 to 24 different chain lengths for single and multiple target states which results in about 130.000 full DMRG runs. We estimate that the calculations consumed overall about 45 CPU years which were provided by 100 parallelized

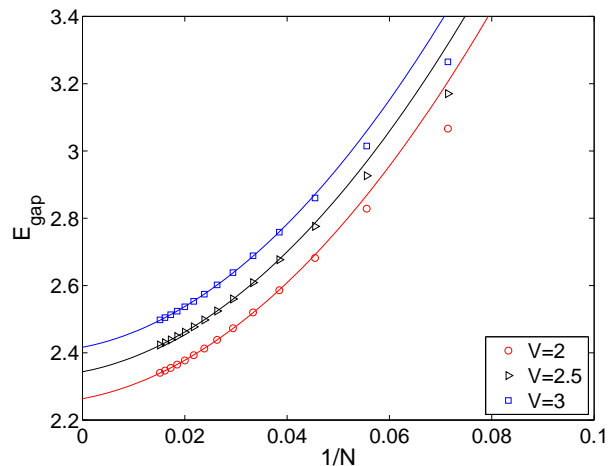


FIG. 3. (Color online) Finite-size scaling of the charge gap  $E_{\text{gap}}$ , calculated for  $t_0 = 2.4 \text{ eV}$ ,  $\alpha = 3.4 \text{ eV/\AA}$ ,  $U = 6 \text{ eV}$ ,  $V = 2.0, 2.5, 3.0 \text{ eV}$ , and  $14 \leq N \leq 66$  sites. The lines are quadratic fits.

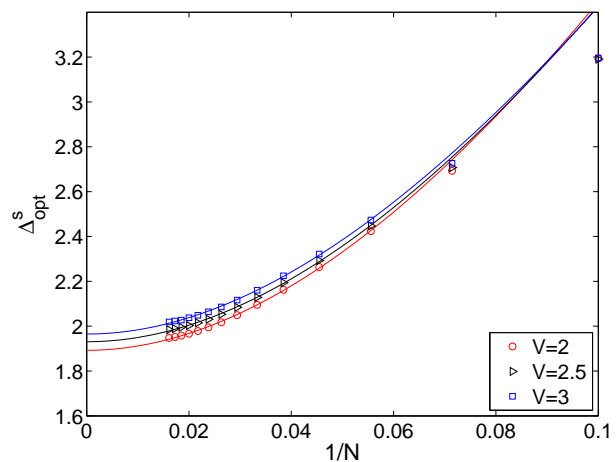


FIG. 4. (Color online) Finite-size scaling of the singlet exciton energy  $E_s$  (optical gap  $\Delta_{\text{opt}}^s$ ), calculated for  $t_0 = 2.4 \text{ eV}$ ,  $\alpha = 3.4 \text{ eV/\AA}$ ,  $U = 6 \text{ eV}$ ,  $V = 2.0, 2.5, 3.0 \text{ eV}$ , and  $10 \leq N \leq 66$  sites. The lines are quadratic fits.

CPUs so that the calculations took some five months in real time.

The PDAs are charge and spin insulators, i.e., the gaps for single-particle, optical, and magnetic excitations are finite. The materials are characterized by finite correlation lengths. Therefore, end effects decay exponentially, and local operators that are calculated in the middle of the chain display a regular behavior as a function of inverse system size. Thus, various quantities that we calculate for finite chain lengths  $N$  can be extrapolated reliably to the thermodynamic limit,  $N \rightarrow \infty$ , by using a second-order polynomial fit.

As an example, in Fig. 3 we show the charge gap calculated for  $t_0 = 2.4$ ,  $\alpha = 3.4 \text{ eV/\AA}$ ,  $U = 6 \text{ eV}$ , and  $V = 2.0, 2.5, 3.0 \text{ eV}$ , as a function of  $1/N$ . As seen from



the figure, the second-order polynomial fits permit a reliable extrapolation but the quadratic curvature becomes dominant for  $N \gtrsim 50$  only. Therefore, a study of long chains is mandatory. The appearance of the inflection point at sizable chain lengths is more pronounced for the gap states than for the single-particle gap. An example, the optical gap, is shown in Fig. 4.

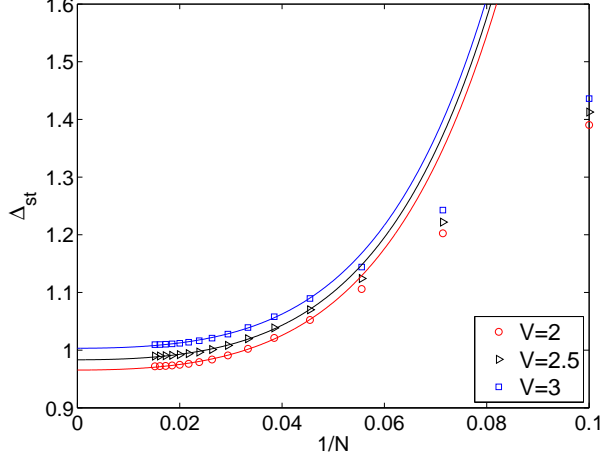


FIG. 5. (Color online) Finite-size scaling of the triplet ground-state energy  $E_T$  (singlet-triplet gap  $\Delta_{st}$ ), calculated for  $t_0 = 2.4$  eV,  $\alpha = 3.4$  eV/Å,  $U = 6$  eV,  $V = 2.0, 2.5, 3.0$  eV, and  $10 \leq N \leq 66$  sites. The lines are quadratic fits.

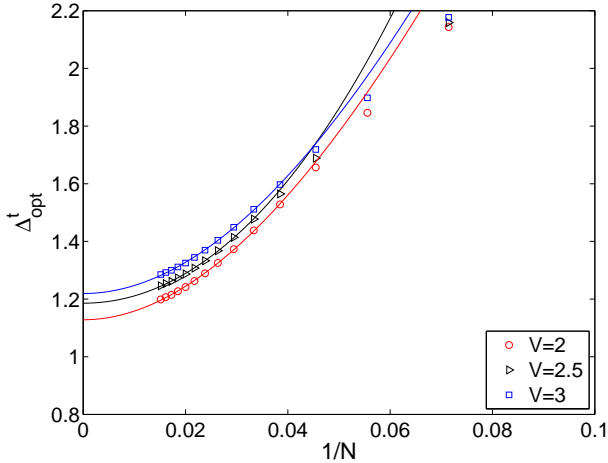


FIG. 6. (Color online) Finite-size scaling of the optical gap in the triplet sector  $\Delta_{opt}^t = E_{T^*} - E_T$ , calculated for  $t_0 = 2.4$  eV,  $\alpha = 3.4$  eV/Å,  $U = 6$  eV,  $V = 2.0, 2.5, 3.0$  eV, and  $14 \leq N \leq 66$  sites. The lines are quadratic fits.

In Figs. 5 and 6 we show finite-size results for the triplet ground-state energy  $E_T$  (singlet-triplet gap  $\Delta_{st}$ ) and for the optical gap in the triplet sector  $\Delta_{opt}^t = E_{T^*} - E_T$ , respectively, for  $t_0 = 2.4$  eV,  $\alpha = 3.4$  eV/Å,  $U = 6$  eV,  $V = 2.0, 2.5, 3.0$  eV. The ground-state energy  $E_T$  in the triplet sector rapidly converges as a function

of inverse system size  $1/N$  because the state is deep in the gap. The energy  $E_{T^*}$  of its optical excitation  $T^*$  is close to the threshold  $E_{gap}$  for single-particle excitations so that long chains must be studied for a reliable extrapolation to the thermodynamic limit. For the scan of our parameter regime as specified in the next section, we limit ourselves to chains of length  $N \leq 66$ . The accuracy of the extrapolation is better than  $\delta E = 0.05$  eV.

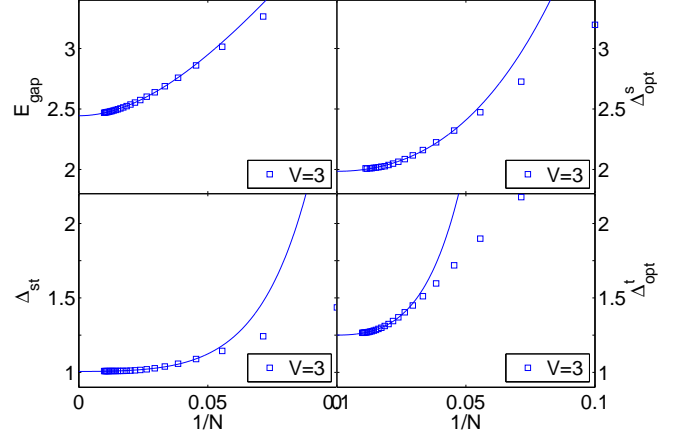


FIG. 7. (Color online) Finite-size scaling of (a) the charge gap  $E_{gap}$ , (b) the optical gap  $\Delta_{opt}^s$ , (c) the singlet triplet gap  $\Delta_{st}$ , and (d) the optical gap in the triplet sector  $\Delta_{opt}^t$ , calculated for the optimal parameter set ( $t_0^* = 2.4$  eV,  $\alpha^* = 3.4$  eV/Å,  $U^* = 6$  eV,  $V^* = 3$  eV), and  $N \leq 102$  sites. The lines are quadratic fits. The extrapolated values are summarized in Tab. I.

Before we detail our optimization of the parameter set in Sect. VIA, we show in Fig. 7 the finite-size scaling of all four gaps for our optimal choice of parameters ( $t_0^* = 2.4$  eV,  $\alpha^* = 3.4$  eV/Å,  $U^* = 6$  eV,  $V^* = 3$  eV) for which we investigate chains with up to  $N = 102$  sites. As can be seen from Fig. 7, the finite-size extrapolation can be done very accurately with an uncertainty of  $\delta E \lesssim 0.01$  eV. The extrapolated values are  $E_{gap} = 2.45$  eV,  $\Delta_{opt}^s = 2.00$  eV,  $\Delta_{st} = 1.00$  eV, and  $\Delta_{opt}^t = 1.25$  eV, see also table I.

## V. PARAMETER REGIME

Before we present our results in Sect. VI, we give arguments for the parameter regime used in our study, as summarized in table III.

### A. Spring constants

At first sight, it seems to be easy to obtain the spring constants  $K$  and  $G$  because they can be inferred from Raman scattering data for short molecules. Unfortunately, the influence of the delocalized  $\pi$  electrons appears to be crucial. For example, early Raman experiments in

ethane,<sup>35</sup>  $\text{H}_3\text{C}-\text{CH}_3$ , give  $K_\sigma^e = 31 \text{ eV}/\text{\AA}^2$  whereas for the single-bond in diacetylene,<sup>36</sup>  $\text{HC}\equiv\text{C}-\text{C}\equiv\text{CH}$ ,  $K_\sigma^{\text{da}} = 45 \text{ eV}/\text{\AA}^2$  is found. In polymers, the situation is equally ambiguous because the theoretical analysis of the same Raman data for poly-acetylene leads to the same set of concurring values<sup>37</sup>  $K_\sigma^{\text{PA},1} = 31 \text{ eV}/\text{\AA}^2$  and  $K_\sigma^{\text{PA},2} = 46 \text{ eV}/\text{\AA}^2$ .<sup>29</sup> In the present work, we investigate the consequences of a strong spring constant for the  $\sigma$ -bond,  $K > 40 \text{ eV}/\text{\AA}^2$ . We plan to present a detailed study of the vibrational properties in the near future.

In order to estimate  $K$  (and  $G$ ), we calculate the optical phonon spectrum from a simple classical model. The carbon atoms of mass  $M = 12u$  in the Lewis structure of Fig. 1 are linked by spring constants of strength  $K$  and  $G = gK$  in the sequence  $(G, K, K, K)$  in the unit cell, corresponding to the  $\sigma$ - $p_y$ -bond and the three  $\sigma$ -bonds. The optical phonons for two-dimensional vibrations of the chain are derived in App. B. There are four positive solutions of the characteristic equation for the phonon frequencies,  $\omega_a < \omega_b = \sqrt{2K/M} < \omega_c < \omega_d$ , where  $\omega_b$  is the resonance frequency of two carbon atoms linked by the spring constant  $K$ .<sup>29</sup> The frequencies  $\omega_{a,c,d}$  are obtained from the zeros of the third-order polynomial

$$p(y) = y^3 - 2(g+2)y^2 + (7/2 + 6g)y - 3g \quad (22)$$

as  $\omega_{a,c,d} = \sqrt{y_{a,c,d}K/M}$ ,  $p(y_{a,c,d}) = 0$ .

In comparison with experiment, see Sect. II B 2, we assign  $\omega_d(g) = \omega_T$  and  $\omega_c(g) = \omega_D$ . From  $(\omega_T/\omega_D)^2 = (0.261/0.181)^2 = 2.079$  we find  $g_0 = 1.547$ ,  $y_d(g_0) = 4.463$ ,  $y_c(g_0) = 2.147$ , and  $y_a(g_0) = 0.4845$ . From  $y_c(g_0) = M\omega_D^2/K$  we obtain  $K = 44.1 \text{ eV}/\text{\AA}^2$  which agrees with results obtained for poly-acetylene chains,<sup>29</sup>  $K_\sigma^{\text{PA},2} = 46 \text{ eV}/\text{\AA}^2$ . In addition, we find  $G = gK = 68.3 \text{ eV}/\text{\AA}^2$  for the  $\sigma$ - $p_y$ -bond. For comparison, the spring constant in ethene (ethylene) was derived as  $K_{\sigma-p_y}^{\text{eth}} = 60 \text{ eV}/\text{\AA}^2$ .<sup>38</sup>

The other two optical phonons have the energies  $\hbar\omega_b = \hbar\sqrt{2K/M} = 0.175 \text{ eV}$ , and  $\hbar\omega_a = \hbar\sqrt{K/M}\sqrt{y_a(g_0)} = 0.086 \text{ eV}$ , respectively. These values are in good agreement with experiment,  $\hbar\omega_b \approx \hbar\omega_{D^*} = 0.155 \text{ eV}$ , and  $\hbar\omega_a \approx \hbar\omega_S = 0.090 \text{ eV}$ , see Sect. II B 2. Note that we use experimental data for comparison which include the influence of the  $\pi$ -electrons whereas for our model calculations we employ bare values for the backbone. The influence of the itinerant  $\pi$  electrons must be calculated self-consistently so that the values for  $K$  and  $G$  need further refinement. This task is left for a future study.

## B. Electron-phonon coupling

Next, we discuss the bare bandstructure for non-interacting electrons and estimate the size of the electron-phonon coupling constant  $\alpha$ .

### 1. Bare bandstructure

The bare bandstructure for the ground state with filled valence bands with energies  $E_{v,2}(k) = -\epsilon_2(k)$  and  $E_{v,1}(k) = -\epsilon_1(k)$  and empty conduction bands with energies  $E_{c,1}(k) = \epsilon_1(k)$  and  $E_{c,2}(k) = \epsilon_2(k)$  is derived in App. C, see eq. (C8). The bare gap is given by  $\Delta^{\text{bare}} = 2\epsilon_1(k=0)$ . The Coulomb interaction enhances all gaps<sup>13</sup> so that the singlet-triplet gap  $\Delta_{\text{st}} = E_T - E_G \approx 1 \text{ eV}$  will be larger than  $\Delta^{\text{bare}}$ . Therefore, the size of the bare band-gap constrains the possible values for the electron-phonon coupling.

In the absence of Coulomb interactions, the values for  $t_s$ ,  $t_d$ , and  $t_t$  must be determined from the minimization of the total ground-state energy per unit cell,

$$e_{\text{tot}}(\delta_d, \delta_t) = e_{\text{kin}}(\delta_d, \delta_t) + e_{\text{pot}}(\delta_d, \delta_t),$$

$$e_{\text{pot}}(\delta_d, \delta_t) = \frac{1}{4\pi t_0 \lambda} \left( \delta_d^2 + g\delta_t^2 + \frac{1}{2}(\delta_t + \delta_d)^2 \right), \quad (23)$$

where  $g = G/K$  and  $\lambda = 2\alpha^2/(\pi t_0 K)$ . The kinetic energy of the electrons is given by

$$e_{\text{kin}}(\delta_d, \delta_t) = -2 \int_{-\pi}^{\pi} \frac{dk}{2\pi} (\epsilon_1(k) + \epsilon_2(k)), \quad (24)$$

where the factor two accounts for the spin degeneracy.

The electron transfer matrix elements  $t_{s,d,t}$  and the distortion corrections  $\delta_{s,d,t}$  are related by  $t_s = t_0 - (\delta_t + \delta_d)/4$ ,  $t_d = t_0 + \delta_d/2$ , and  $t_t = t_0 + \delta_t/2 + \delta^e/2$ . Here, we used the fact that  $2\delta_s + \delta_d + \delta_t = 0$  because the length of the unit cell is not changed by the intrinsic distortion. The strength of the extrinsic dimerization  $\delta^e$  follows from the solution of eq. (A6) of App. A for  $U = V = 0$ ,

$$\frac{\delta^e(U = V = 0)}{\pi t_0 \lambda} = -\frac{8T_1(\delta^e)}{2\epsilon_0(\delta^e)} = \frac{8T_1(\delta^e)}{4T_1(\delta^e)} = 2 \quad (25)$$

so that  $\delta^e(U = V = 0) = 4\alpha^2/K$ .

The numerical minimization of  $e_{\text{tot}}(\delta_d, \delta_t)$ , eq. (23), leads to the somewhat surprising result that the bare gap  $\Delta^{\text{bare}}(t_0, \alpha)$  very weakly depends on  $t_0$ . For  $\alpha = 3.5 \text{ eV}/\text{\AA}$ ,  $K = 44 \text{ eV}/\text{\AA}^2$ , and  $G = 68 \text{ eV}/\text{\AA}^2$ , we find that  $\Delta^{\text{bare}}(2, 3.5) = 0.878 \text{ eV}$  and  $\Delta^{\text{bare}}(2.4, 3.5) = 0.835 \text{ eV}$ ; it even decreases slightly with increasing  $t_0$ . In contrast, the bare band-gap strongly increases as a function of  $\alpha$ . For  $t_0 = 2.4 \text{ eV}$ ,  $K = 44 \text{ eV}/\text{\AA}^2$ , and  $G = 68 \text{ eV}/\text{\AA}^2$ , we find  $\Delta^{\text{bare}}(2.4, 3.4) = 0.776 \text{ eV}$  and  $\Delta^{\text{bare}}(2.4, 3.6) = 0.897 \text{ eV}$ . The bare band-gap becomes larger than  $\Delta_{\text{st}} = 1 \text{ eV}$  for  $t_0 = 2.4 \text{ eV}$  and  $\alpha = 3.8 \text{ eV}/\text{\AA}$ . Therefore, we must use smaller values for  $\alpha$  as derived and used previously.<sup>18,29</sup>

### 2. Intrinsic and extrinsic Peierls distortion

In poly-acetylene (PA), the mobile  $\pi$ -electrons dimerize the chain. This intrinsic Peierls effect results in a measured bond length alternation of  $\Delta r = 0.04 \text{\AA}$ , i.e., long

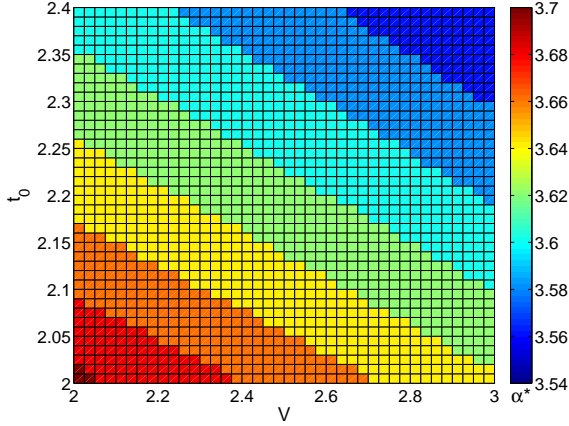


FIG. 8. (Color online) Regions in the parameter space  $t_0$ - $V$  which lead to  $R_1 = 1.25 \text{ \AA}$  for  $U = 6 \text{ eV}$ . The color coding gives the appropriate value for  $\alpha$ .

and short bonds of length  $r_s^{\text{PA}} = 1.44 \text{ \AA}$  and  $r_d^{\text{PA}} = 1.36 \text{ \AA}$  alternate along the chain.<sup>39</sup> Almost the same amount of alternation in  $r_s$  and  $r_d$  is seen in PDAs, see Sect. II A 2. Previous DMRG studies<sup>18</sup> lead to  $\Delta r = 0.03 \text{ \AA}$ .

When we assume that the intrinsic Peierls effect affects the triple bond in the same way as the double bond, we come to the conclusion that the length  $R_1$  of the  $\sigma$ - $p_y$ -bond before the intrinsic dimerization is  $R_1 \approx 1.25 \text{ \AA}$  assuming  $r_t = 1.21 \text{ \AA}$ . Therefore, the extrinsic dimerization due to the  $p_y$ -bond accounts for  $r_0 - R_1 = \delta^e/(2\alpha) = 0.15 \text{ \AA}$ . For non-interacting electrons, we have  $\delta^e(U = V = 0) = 4\alpha^2/K$ , independent of  $t_0$ . Thus, we arrive at the estimate  $\alpha \approx 0.15 \text{ \AA}(K/2)$  which gives  $\alpha \approx 3.3 \text{ eV/\AA}$  for  $K = 44 \text{ eV/\AA}^2$ .

Even in the presence of Coulomb interactions, the calculation of  $\delta^e$  is simple because it requires the solution of a two-site problem only, see App. A. Therefore, a complete parameter scan is readily accomplished. As we shall argue below, the on-site Coulomb repulsion  $U$  is quite substantial. Therefore, in Fig. 8 we show parameter regions in  $(t_0, \alpha, V)$  for  $U = 6 \text{ eV}$  that correspond to  $\delta^e/(2\alpha) = 0.15 \text{ \AA}$ . As compared to non-interacting electrons, the electron-phonon coupling  $\alpha$  has to be increased by some 10% to generate the same extrinsic Peierls dimerization for the interacting two-site system. This indicates that the Coulomb interaction makes the bonds noticeably stiffer. In order to account for this effect, our spring constant  $K$  from Sect. V A should be reduced by at least ten percent; a more thorough scan for the  $K$ -parameter will be done in a future study.

Fig. 8 shows that the dependence on  $t_0$  and  $V$  is rather weak: it is mostly the Peierls coupling  $\alpha$  that determines the size of the bond length shift. From the data in Fig. 8 we conclude that  $\alpha \approx (3.5 \pm 0.1) \text{ eV/\AA}$  is a reasonable starting point, whereby we compensate our somewhat too large spring constant  $K$ .

### C. Coulomb parameters

Previous studies<sup>10,11,16,18</sup> succeeded to reproduce the charge gap and the energy of the singlet exciton. However, the complexity of the in-gap states could not be recovered. In particular, the splitting  $\Delta_{\text{st}}$  of the singlet and triplet ground states cannot be reproduced as it comes out substantially too high. Moreover, in previous approaches no dark singlet states have been found that lie energetically below the singlet exciton.

The energetic positions of the states T and  $X_{1,2}$  are a clear signal of substantial electronic correlations induced by the Hubbard interaction  $U$ . Our initial calculations with small ratios  $U/V$  put T and  $X_{1,2}$  too high in energy as compared to experiment.<sup>40</sup> As we shall show in the next section, we find a reasonably good description of the level scheme in Fig. 2 only for substantial  $U$  and comparably small  $V$ ,  $5 \text{ eV} \leq U \leq 6 \text{ eV}$  and  $2 \text{ eV} \leq V \leq 3 \text{ eV}$ , as indicated in table III, so that  $U/V = \kappa \approx 2$  holds. Note that we included the dielectric constant  $\epsilon_d$  explicitly in the Ohno potential (6) because we treat chains immersed in their monomer matrix.

Substantial values for the Coulomb interaction were advanced by Chandross and Mazumdar<sup>20</sup> as a result of their model study of poly-phenylene-vinylene (PPV) thin films. In order to describe the linear and non-linear optical properties of PPV, they proposed  $U_{\text{CM}} = 8 \text{ eV}$  with  $U_{\text{CM}}/V_{\text{CM}} = \kappa = 2$ .<sup>20,41</sup> Note, however, that these authors worked with fixed lattice parameters, i.e., without lattice relaxations for the excitations, and employed an approximation (single configuration interaction, SCI) to calculate optical excitations.

The bare bandwidth in our calculations is  $W \approx 4t_0 \gtrsim 9 \text{ eV}$  which still is larger than the on-site interaction. Therefore, the system is still far from the spin-Peierls limit. At the same time, however, the correlations are strong enough to impede weak-coupling approaches.<sup>13</sup>

## VI. RESULTS

First, we scan our parameter space and determine our best parameter set  $(t_0, \alpha, U, V)$ . Next, we analyze the energy levels of optically dark in-gap states and comment on the lattice parameters.

### A. Optimization of the parameter set

For each choice of the parameter set  $(t_0, \alpha, U, V)$ , we calculate the ground-state energies at half band-filling and one additional particle, and the energy of the three excited state S, T, and T\* at half band-filling from which we determine the four gaps  $E_{\text{gap}}$ ,  $\Delta_{\text{opt}}^s$ ,  $\Delta_{\text{st}}$ , and  $\Delta_{\text{opt}}^t$  for systems with size  $10 \leq N \leq 66$ . The lattice geometry of all states is relaxed, see Sect. IV. We performed calculations for  $(t_0, \alpha, U, V)$  for a broad range of parameters using small system sizes up to  $N = 30$  sites. For the optimal

range ( $t_0 = 2.0, 2.2, 2.3, 2.4$  eV,  $\alpha = 3.4, 3.5, 3.6$  eV/Å,  $U = 5.0, 5.5, 6.0$  eV,  $V = 2.0, 2.5, 3.0$  eV) we investigated systems with up to  $N = 66$  sites, i.e., we address altogether 108 different parameter sets.

As an example, in Fig. 9 we show the extrapolated energies for fixed ( $t_0 = 2.4$  eV,  $U = 6.0$  eV), as a function of  $V = 2.0, 2.5, 3.0$  eV for the three parameters  $\alpha = 3.4, 3.5, 3.6$  eV/Å. As expected for our small parameter window, we observe a fairly linear dependence of the gaps on the parameters  $V$  and  $\alpha$ . It is seen that not all the gaps can be reproduced perfectly with a single parameter set. In general, for fixed ( $t_0, U$ ), the optical gap in the triplet sector,  $\Delta_{\text{opt}}^t = E_{T^*} - E_T$  requires larger values for ( $\alpha, V$ ) than the other gaps. Therefore, we have to compromise to find a good parameter set.

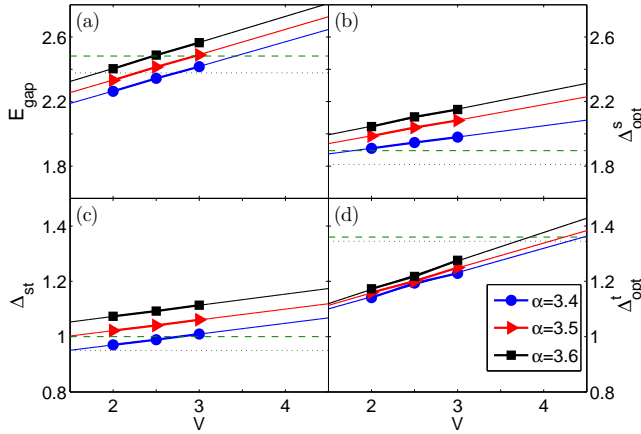


FIG. 9. (Color online) Extrapolated energies as a function of  $V$  for  $\alpha = 3.4, 3.5, 3.6$  eV/Å for fixed ( $t_0 = 2.4$  eV,  $U = 6.0$  eV). The horizontal lines give the experimental results for 3BCMU (green dashed) and 4BCMU (black dotted).

To this end, we define  $V_i^*$  as the value  $V$  for a given ( $t_0, \alpha, U$ ) which reproduces the experimental gaps  $i$  ( $i = 1, 2, 3, 4$  for  $E_{\text{gap}}, \Delta_{\text{opt}}^s, \Delta_{\text{st}}, \Delta_{\text{opt}}^t$ ) for 3BCMU and 4BCMU from table I. Then, we calculate the joint standard deviation  $\sigma(t_0, \alpha, U)$  from

$$[\sigma(t_0, \alpha, U)]^2 = \frac{1}{6} \sum_{i>j} [(V_i^* - V_j^*)/\text{eV}]^2. \quad (26)$$

The optimal parameter set minimizes the spread  $\sigma$ . The results for  $\sigma(t_0, \alpha, U)$  are shown in table IV for 3BCMU and for 4BCMU in table V, respectively.

The two tables IV and V indicate that the best set for both 3BCMU and 4BCMU is ( $t_0 = 2.4$  eV,  $\alpha = 3.4$  eV/Å,  $U = 6$  eV). Then, a look at Fig. 9 shows that  $V = 3$  eV is the best value for which we have data available. Therefore, we shall use the set ( $t_0^* = 2.4$  eV,  $\alpha^* = 3.4$  eV/Å,  $U^* = 6$  eV,  $V^* = 3$  eV) as our optimal parameter set. The trend shows that  $\alpha$  might even be a bit smaller,  $\alpha \lesssim 3.4$  eV/Å, and  $t_0$  a bit larger,  $t_0 \gtrsim 2.4$  eV, for the optimal case. We plan to perform a more system-

$U = 5.0$ eV	$t_0/\text{eV}$		
	2.0	2.2	2.4
$\alpha = 3.4$ eV/Å	1.96	2.79	3.22
$\alpha = 3.5$ eV/Å	<b>1.68</b>	3.12	3.67
$\alpha = 3.6$ eV/Å	2.66	3.63	4.11

$U = 5.5$ eV	$t_0/\text{eV}$		
	2.0	2.2	2.4
$\alpha = 3.4$ eV/Å	1.91	<b>1.63</b>	2.28
$\alpha = 3.5$ eV/Å	1.96	2.14	2.85
$\alpha = 3.6$ eV/Å	2.53	2.63	3.37

$U = 6.0$ eV	$t_0/\text{eV}$		
	2.0	2.2	2.4
$\alpha = 3.4$ eV/Å	14.07	1.95	<b>1.55</b>
$\alpha = 3.5$ eV/Å	3.56	2.06	2.11
$\alpha = 3.6$ eV/Å	3.59	2.91	3.67

TABLE IV. Spread  $\sigma$  as a function of ( $t_0, \alpha, U$ ) for 3BCMU where the experimentally observed gaps are given by  $E_{\text{gap}} = 2.482$  eV,  $\Delta_{\text{opt}}^s = 1.896$  eV,  $\Delta_{\text{st}} = 1.0$  eV, and  $\Delta_{\text{opt}}^t = 1.360$  eV. The three best sets ( $t_0, \alpha, U$ ) are printed in **bold**.

$U = 5.0$ eV	$t_0/\text{eV}$		
	2.0	2.2	2.4
$\alpha = 3.4$ eV/Å	2.42	3.19	3.66
$\alpha = 3.5$ eV/Å	<b>2.30</b>	3.65	4.16
$\alpha = 3.6$ eV/Å	3.36	4.17	4.58

$U = 5.5$ eV	$t_0/\text{eV}$		
	2.0	2.2	2.4
$\alpha = 3.4$ eV/Å	2.85	<b>2.31</b>	2.91
$\alpha = 3.5$ eV/Å	2.67	2.87	3.45
$\alpha = 3.6$ eV/Å	3.37	3.34	3.96

$U = 6.0$ eV	$t_0/\text{eV}$		
	2.0	2.2	2.4
$\alpha = 3.4$ eV/Å	17.89	2.51	<b>2.15</b>
$\alpha = 3.5$ eV/Å	3.96	2.56	2.68
$\alpha = 3.6$ eV/Å	4.07	3.64	5.12

TABLE V. Spread  $\sigma$  as a function of ( $t_0, \alpha, U$ ) for 4BCMU where the experimentally observed gaps are given by  $E_{\text{gap}} = 2.378$  eV,  $\Delta_{\text{opt}}^s = 1.810$  eV,  $\Delta_{\text{st}} = 0.95$  eV, and  $\Delta_{\text{opt}}^t = 1.345$  eV. The three best sets ( $t_0, \alpha, U$ ) are printed in **bold**.

atic estimate for the optimal parameter set in the near future.

For our optimal parameter set ( $t_0^* = 2.4$  eV,  $\alpha^* = 3.4$  eV/Å,  $U^* = 6$  eV,  $V^* = 3$  eV), the corresponding theoretical values for the excitation energies are  $E_{\text{gap}} = 2.45$  eV,  $\Delta_{\text{opt}}^s = 2.00$  eV,  $\Delta_{\text{st}} = 1.00$  eV, and  $\Delta_{\text{opt}}^t = 1.25$  eV. They are also given in table I.

## B. Optically dark in-gap triplet states

In the triplet sector, we find a series of optically dark states  $Y_l$  ( $l = 1, 2, 3, 4$ ) at energies just above the triplet ground state. As indicated in Fig. 2, the optically dark

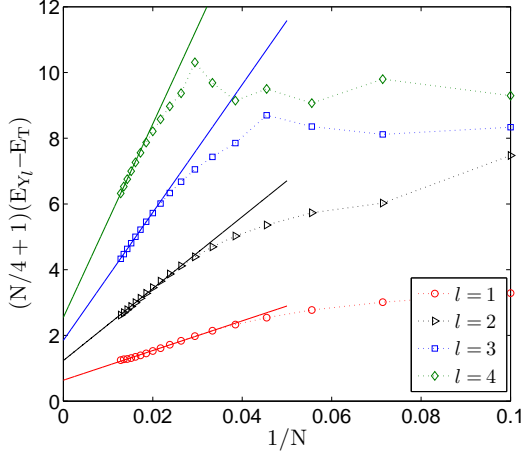


FIG. 10. (Color online) Scaled excitation energies of the first four triplet states,  $D_l = (N/4 + 1)(E_{Y_l} - E_T)$ , as a function of inverse system size  $1/N$  for  $10 \leq N \leq 78$  and  $(t_0^* = 2.4 \text{ eV}, \alpha^* = 3.4 \text{ eV}, U^* = 6 \text{ eV}, V^* = 3 \text{ eV})$ . The crossings of the ordinate are equidistant,  $D_1 = 0.637 \text{ meV}$ ,  $D_2 = 1.235 \text{ meV}$ ,  $D_3 = 1.851 \text{ meV}$ , and  $D_4 = 2.548 \text{ meV}$ , indicating a linear dispersion relation for the excitations.

triplet states  $Y_l$  open decay channels for the states  $X_1$  and  $X_2$ .

The structure of the optically dark in-gap triplet states is also interesting from a theoretical point of view. In a band picture, the triplet ground state with spin component  $S^z = 1$  consists of a hole in the  $\downarrow$  valence band and an electron in the  $\uparrow$  conduction band, both at momentum  $k = 0$ . Close in energy are the corresponding excitations at finite but small momentum  $k$ . The dispersion of these excitations is quadratic as a function of  $k$ .

In the interacting case, these excitations may form a spin-flip density wave with momentum  $q$  whose dispersion relation at low-energy is given by

$$\epsilon_{\text{sf}}(q) = c_{\text{sf}} q, \quad (27)$$

where  $c_{\text{sf}}$  is the (sound) velocity. For finite chains, we have quantized quasi-momenta,  $q_l = \pi l / [(N/4 + 1)d]$  ( $l = 1, 2, \dots$ ), where  $d$  is the length of the unit cell. Therefore, the levels  $Y_l$  should obey

$$E_{Y_l} - E_T = \epsilon_{\text{sf}}(q_l) + \frac{\alpha_l}{N^2} + \dots, \quad (28)$$

$$\left(\frac{N}{4} + 1\right)(E_{Y_l} - E_T) = c_{\text{sf}} \frac{l\pi}{d} + \frac{\alpha_l}{N} + \dots \quad (29)$$

We confirm this hypothesis in Fig. 10 where we show  $(N/4 + 1)(E_{Y_l} - E_T)$  as a function of  $1/N$ . As seen from the figure, the energy differences scale to a finite value linearly in  $1/N$ . Moreover, the extrapolated values are equidistant from which we can read off  $\Delta_{\text{sf}} \equiv c_{\text{sf}}\pi/d = 0.625 \text{ meV}$ . Using  $d = 4.9 \text{ \AA}$  we thus estimate the velocity for the spin-flip density excitations as  $c_{\text{sf}} = 148 \text{ m/s}$ . For localized spin models, we have

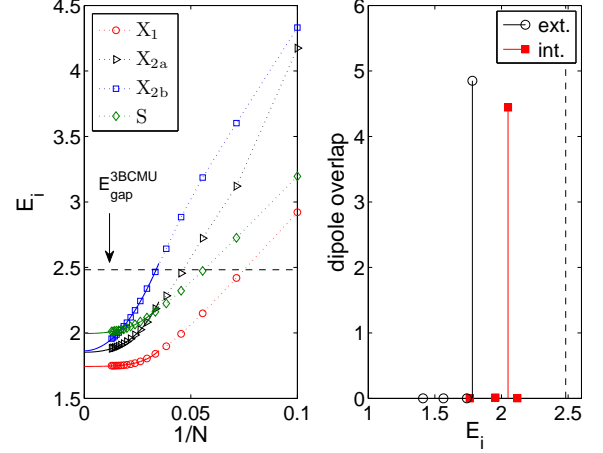


FIG. 11. (Color online) (a) Energies of the lowest singlet states as a function of inverse system size  $1/N$  for  $10 \leq N \leq 78$  for  $(t_0^* = 2.4 \text{ eV}, \alpha^* = 3.4 \text{ eV}, U^* = 6 \text{ eV}, V^* = 3 \text{ eV})$ . After the extrapolation, the states  $X_{2a}$  and  $X_{2b}$  are essentially degenerate,  $E_{X_1} = 1.744 \text{ eV}$ ,  $E_{X_{2a}} = 1.853 \text{ eV}$ ,  $E_{X_{2b}} = 1.863 \text{ eV}$ , and  $E_S = 1.995 \text{ eV}$ . The horizontal dashed line gives the value for the charge gap in 3BCMU. (b) Overlap intensity of the dipole operator for spin-singlet in-gap states after the extrinsic and the intrinsic relaxation for  $N = 46$  sites.

$c_J \approx J(d/4)$  so that, approximating  $c_J \approx c_{\text{sf}}$ , the effective magnetic interaction in our system is of the order of one meV,  $J \approx (4/\pi)\Delta_{\text{sf}} = 0.8 \text{ meV}$ .

### C. Optically dark in-gap singlet states

In Fig. 11a we show the (relaxed) excitation energies for the four energetically lowest singlet states as a function of  $1/N$  for  $(t_0^* = 2.4 \text{ eV}, \alpha^* = 3.4 \text{ eV/\AA}, U^* = 6 \text{ eV}, V^* = 3 \text{ eV})$ . For our optimal parameter set, there are at least three optically dark singlet states below the singlet exciton. We extrapolate  $E_{X_1} = 1.744 \text{ eV}$  which is about  $0.25 \text{ eV}$  higher than estimated from experiment, see table I. This indicates that the local correlations could still be larger than  $U = 6 \text{ eV}$ . Note, however, that the absolute positions of  $X_1$  and  $X_2$  have not been determined experimentally for nBCMU but it is known from pump-probe spectroscopy<sup>3</sup> that there are (at least) two optically dark singlet states below the singlet exciton.

The next two dark in-gap singlets are almost degenerate in energy,  $E_{X_{2a}} = 1.853 \text{ eV}$  and  $E_{X_{2b}} = 1.863 \text{ eV}$ . They lie below the singlet exciton, as seen in experiment, but about  $0.15 \text{ eV}$  higher than estimated in table I. Fig. 11b shows the dipole overlap<sup>16</sup> for the four singlet states  $X_1$ ,  $X_{2a}$ ,  $X_{2b}$ , and  $S$  at chain length  $N = 46$ . Only the exciton  $S$  has a finite dipole overlap. Note the energy shift of all in-gap states due to the intrinsic Peierls effect. The Peierls shift amounts to several tenths of an eV.

As in the triplet sector, we employ the band picture at fixed particle number to view the elementary excita-



tions of the ground state as a hole in the valence band and an electron in the conduction band. In a Wannier picture, the electron-electron interaction forms bound states from these pairs, such as  $X_1$ , the lowest-lying  $A_g$  singlet, and  $S$ , the singlet exciton with  $B_u$  symmetry. Apart from these bound states, there should be a continuum of scattering states. The degeneracy of the states  $X_{2a}$  and  $X_{2b}$  indicates that they are near the threshold to the X-continuum. Indeed, two-photon absorption above  $E_f \approx 2.0$  eV excites states that can fission into two triplets.<sup>3</sup> Unfortunately, it takes a significant amount of CPU time in our DMRG approach to target more than four in-gap singlet states simultaneously so that a more detailed investigation of the in-gap spectrum remains an open problem.

#### D. Lattice parameters

Finally, we show results for the lattice constants in Fig. 12. For our optimal set of parameters, the extrapolated values are  $r_s = 1.425$  Å,  $r_d = 1.373$  Å, and  $r_t = 1.239$  Å, for the single, double, and triple bond, respectively. When compared to the experimental values for PDA single crystals given in Sect. II A, the values for the single and double bonds are rather good but the triple bond is too large. This can also be seen from the size of the unit cell. Given the Lewis structure of Fig. 1, the unit cell in chain direction has the length  $d$  with  $d^2 = r_d^2 + (2r_s + r_t)^2 - 2r_d(2r_s + r_t)\cos(\varphi_1)$ . Using  $\varphi_1 = 120^\circ$ , this results in  $d = 4.92$  Å which is slightly larger than the experimental values for 3BCMU chains,  $d_{3BCMU} = 4.89$  Å.<sup>3</sup>

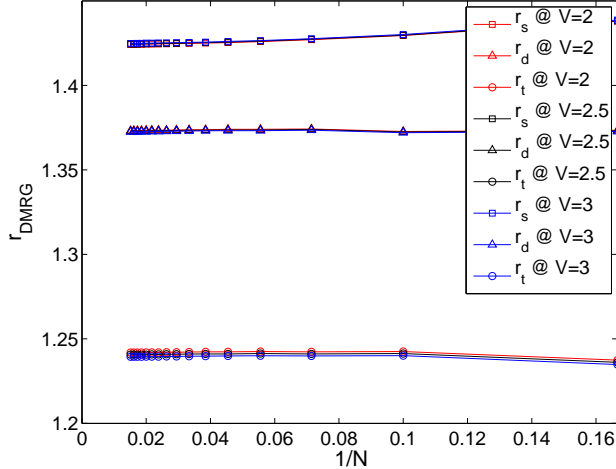


FIG. 12. (Color online) Atomic distances  $r_s$ ,  $r_d$  and  $r_t$  for the single, double, and triple bonds in the chain center as function of inverse system size  $1/N$  for  $6 \leq N \leq 66$  for  $(t_0 = 2.4 \text{ eV}, \alpha = 3.4 \text{ eV/\AA}, U = 6 \text{ eV})$ , and  $V = 2.0, 2.5, 3.0 \text{ eV}$ . The extrapolated values for the best parameter set ( $V = 3 \text{ eV}$ ) are  $r_s = 1.425$  Å,  $r_d = 1.373$  Å, and  $r_t = 1.239$  Å.

The comparison shows that the spring constants  $K$  and  $G$  are too large and/or the electron-phonon coupling constant  $\alpha$  is too small. Consequently, the spring constants  $K$ ,  $G$  should be included as parameters in the optimization procedure.

## VII. CONCLUSIONS

### A. Parameter values

In our study we use quite sizable values for the Coulomb parameters. Substantial values for the Hubbard interaction,  $U_{CM} = 8 \text{ eV}$ , were used by Chandross, Mazumdar et al. in their studies of the optical properties of poly-phenylene-vinylene (PPV) thin films.<sup>20</sup> For PDA chains immersed in their monomer matrix, we find  $U = 6 \text{ eV}$  and confirm their previous result for the ratio between  $U$  and  $V$ ,  $U_{CM}/V_{CM} = \kappa = U/V = 2$ .<sup>20,41</sup> Note that we additionally screen the long-range part of the Coulomb interaction by the dielectric constant of the monomer matrix,  $\epsilon_d = 2.3$ . A further increase of the Hubbard interaction beyond  $U = 6 \text{ eV}$  would be problematic, as can be seen from Fig. 13a. For fixed  $t_0$  and  $\alpha$ , the spread of the gaps increases with increasing  $U$ . In particular, the calculated singlet-exciton energy would deviate significantly from its experimental value. Moreover, the number of dark singlet states below the exciton would become larger than expected from experiment.

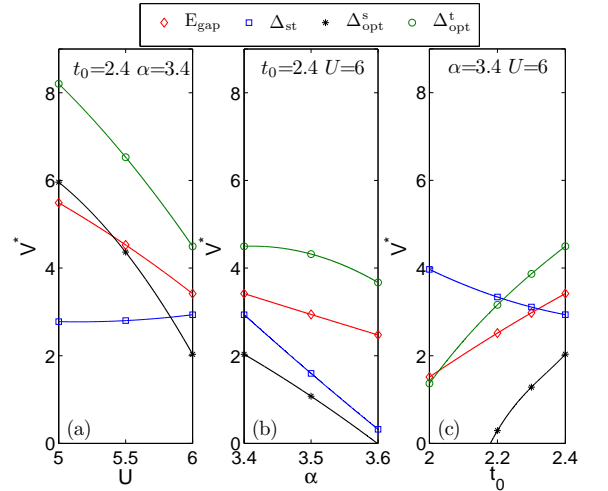


FIG. 13. (Color online) Optimal values  $V_i^*$  for the four gaps  $E_{\text{gap}}$ ,  $\Delta_{\text{opt}}^s$ ,  $\Delta_{\text{st}}$ , and  $\Delta_{\text{opt}}^t$  (a) as a function of  $U$  for  $t_0 = 2.4 \text{ eV}$  and  $\alpha = 3.4 \text{ eV/\AA}$ , (b) as a function of  $\alpha$  for  $t_0 = 2.4 \text{ eV}$  and  $U = 6 \text{ eV}$ , and (c) as a function of  $t_0$  for  $U = 6 \text{ eV}$  and  $\alpha = 3.4 \text{ eV/\AA}$ .

For fixed  $t_0 = 2.4 \text{ eV}$  and  $U = 6 \text{ eV}$ , a change from  $\alpha = 3.4 \text{ eV/\AA}$  would increase the spread in the gaps, as can be seen from Fig. 13b. Therefore, we advocate an electron-phonon coupling strength which is some 15%

smaller than the value proposed by Ehrenfreund et al.,  $\alpha_E = 4.0 \text{ eV}/\text{\AA}$ .<sup>29</sup>

In the literature, typical values for the electron transfer integral are  $t_0 = 2.5 \text{ eV}$ <sup>28,37</sup> and  $t_0 = 2.4 \text{ eV}$ <sup>20,41</sup>. Our work indicates that a readjustment of the bare electron transfer integral is not necessary for nBCMU. This can be seen from Fig. 13c, where the spread of  $V_i$  increases for both smaller and larger  $t_0$ .

## B. Outlook

Our study can be extended in several directions. First, the strength of the spring constants  $K$  and  $G$  must be determined self-consistently. In this way, a better agreement between theory and experiment for the lattice parameters can be obtained.

Second, the parameter search in the four-dimensional space  $(t_0, \alpha, U, V)$  can be optimized by performing a smooth interpolation between the 81 data sets which we have investigated numerically thus far. Moreover, the present analysis does not distinguish between various ligand types (3BCMU, 4BCMU). The differences are partly due to strain, and a distinction between PDAs must therefore be incorporated in the lattice parameters. In addition, different side-groups introduce (small) electrostatic potential at the carbon atoms which are linked to the side groups. Our numerical analysis shows that the influence of an electrostatic potential of the order of  $\epsilon_i \leq 0.3 \text{ eV}$  at the side-group sites changes the spectra by  $\delta E \lesssim 0.05 \text{ eV}$  so that this contribution can be ignored to first approximation.

Third, for an optimal parameter set it is interesting to study the properties of the ground and excited states in more detail. For example, the lattice structure of the exciton (polaron-exciton) and its polarizability can be calculated<sup>16,42</sup> and be compared with experiment. Moreover, further in-gap states should be address, e.g., the spin-2 ground state  $1^5A_g$ , or a second singlet exciton  $2^1B_u^-$ .

These tasks are left for a future study.

## Acknowledgments

We thank Gerhard Weiser, Michel Schott, and Benjamin Janesko for useful discussions. This work was supported in part by the Deutsche Forschungsgemeinschaft through GRK 790, and by the Hungarian Research Fund (OTKA) Grants Nos. K 100908 and K 73455. Ö.L. acknowledges support from the Alexander-von-Humboldt foundation and from ETH Zurich during his time as a visiting professor.

## Appendix A: Extrinsic dimerization

Following Ref. [18], we diagonalize the two-site Peierls-Hubbard-Ohno model in the spin singlet sector to derive the ground-state energy. To this end we consider the two states in site representation

$$\begin{aligned} |1\rangle &= \sqrt{\frac{1}{2}} \left( \hat{c}_{1,\uparrow}^+ \hat{c}_{2,\downarrow}^+ - \hat{c}_{1,\downarrow}^+ \hat{c}_{2,\uparrow}^+ \right) |\text{vac}\rangle, \\ |2\rangle &= \sqrt{\frac{1}{2}} \left( \hat{c}_{1,\uparrow}^+ \hat{c}_{1,\downarrow}^+ + \hat{c}_{2,\uparrow}^+ \hat{c}_{2,\downarrow}^+ \right) |\text{vac}\rangle. \end{aligned}$$

In the subspace  $S = 0$ , the Hamilton matrix of the electronic problem has the entries  $(H_e)_{i,j} = \langle i | \hat{H}_e | j \rangle$  ( $i, j = 1, 2$ ). A short calculation gives

$$\underline{H_e} = \begin{pmatrix} -U/2 & -2T_1(\delta^e) \\ -2T_1(\delta^e) & U/2 - V(\delta^e) \end{pmatrix}, \quad (\text{A1})$$

where

$$\begin{aligned} V(\delta^e) &= \frac{V/\epsilon_d}{\sqrt{1 + \beta(R_1(\delta^e)/\text{\AA})^2}}, \\ R_1(\delta^e) &= r_0 - \frac{\delta^e}{2\alpha}, \quad T_1(\delta^e) = t_0 + \frac{\delta^e}{2}. \end{aligned} \quad (\text{A2})$$

$R_1(\delta^e)$  is the length of the  $\sigma$ - $p_y$  double bond,  $T_1(\delta^e)$  is the corresponding electron transfer amplitude,  $U$  is the strength of the electrons' local Coulomb repulsion, and  $V(\delta^e)$  is their interaction on neighboring sites. Note that in Ref. [18], the unshifted energies were used, i.e., the previous expressions follow from ours after an energy shift by  $U/2 + V(\delta^e)$ .

The ground-state energy  $\epsilon_0$  of the two-electron system follows from the diagonalization of the matrix (A1) as

$$\epsilon_0(\delta^e) = -\frac{1}{2} \left( V(\delta^e) + \sqrt{[U - V(\delta^e)]^2 + [4T_1(\delta^e)]^2} \right). \quad (\text{A3})$$

Now that we know the ground-state energy of the electronic Hamiltonian explicitly, we do not have to invoke the Hellmann-Feynman theorem in order to determine the optimal values for the electron transfer amplitudes  $\delta^e$ . Instead, we directly minimize the total ground-state energy

$$E_0(\delta^e) = \epsilon_0(\delta^e) + \frac{(\delta^e)^2}{4\pi t_0 \lambda} \quad (\text{A4})$$

with respect to  $\delta^e$  ( $\lambda = 2\alpha^2/(\pi K t_0)$ ). We set

$$V'(\delta^e) = \frac{\partial V(\delta^e)}{\partial \delta^e} = \frac{V\beta R_1(\delta^e)}{2\alpha\epsilon_d\text{\AA}^2} \frac{1}{[1 + \beta(R_1(\delta^e)/\text{\AA})^2]^{3/2}}. \quad (\text{A5})$$

Therefore, the optimization of the electron-lattice problem for two carbon atoms with a double bond leads to the implicit equation

$$\frac{\delta^e}{\pi t_0 \lambda} = \frac{[2\epsilon_0(\delta^e) + U]V'(\delta^e) - 8T_1(\delta^e)}{2\epsilon_0(\delta^e) + V(\delta^e)}, \quad (\text{A6})$$

which is solved iteratively.

## Appendix B: Optical phonons

Assuming the Lewis structure of Fig. 1, the position of the atoms in the unit cell are denoted by the two-dimensional vectors  $\vec{A}_l$ ,  $\vec{B}_l$ ,  $\vec{C}_l$ , and  $\vec{D}_l$  for  $l = 1, \dots, L = N/4$ . Their equilibrium positions are denoted as  $\vec{A}_{l,0}$ ,  $\vec{B}_{l,0}$ ,  $\vec{C}_{l,0}$ , and  $\vec{D}_{l,0}$ . The PDA structure implies  $\vec{B}_{l,0} - \vec{A}_{l,0} = \vec{D}_{l,0} - \vec{C}_{l,0} = r_s \vec{e}_x$ ,  $\vec{C}_{l,0} - \vec{B}_{l,0} = r_t \vec{e}_x$ , and  $\vec{A}_{l+1,0} - \vec{D}_{l,0} = r_d (\cos(\phi) \vec{e}_x - \sin(\phi) \vec{e}_y)$  for the singlet, triplet, and doublet bonds, where  $\phi = 180^\circ - \varphi_1 = 60^\circ$ .

### 1. Lagrange function

We shall treat the atomic motions classically. For convenience, we use periodic boundary conditions,  $L+1 \equiv 1$ .

The kinetic energy of the atoms is given by

$$T = \frac{M}{2} \sum_{l=1}^L \left[ \left( \dot{\vec{A}}_l \right)^2 + \left( \dot{\vec{B}}_l \right)^2 + \left( \dot{\vec{C}}_l \right)^2 + \left( \dot{\vec{D}}_l \right)^2 \right]. \quad (\text{B1})$$

In the spring-constant model, the atoms' potential energy is approximated by ( $g = G/K$ )

$$V = \frac{K}{2} \sum_{l=1}^L \left[ \left( \left| \vec{B}_l - \vec{A}_l \right| - r_s \right)^2 + g \left( \left| \vec{C}_l - \vec{B}_l \right| - r_t \right)^2 + \left( \left| \vec{D}_l - \vec{C}_l \right| - r_s \right)^2 + \left( \left| \vec{A}_{l+1} - \vec{D}_l \right| - r_d \right)^2 \right]. \quad (\text{B2})$$

To second order in the displacement  $\vec{\delta x} = \vec{x} - \vec{x}_0$  we can write

$$(|\vec{x}| - |\vec{x}_0|)^2 \approx \left( \vec{\delta x} \cdot \vec{x}_0 / |\vec{x}_0| \right)^2. \quad (\text{B3})$$

We define the (small) displacements  $\vec{a}_l = \vec{A}_l - \vec{A}_{l,0} = a_l^x \vec{e}_x + a_l^y \vec{e}_y$ ,  $\vec{b}_l = \vec{B}_l - \vec{B}_{l,0} = b_l^x \vec{e}_x + b_l^y \vec{e}_y$ ,  $\vec{c}_l = \vec{C}_l - \vec{C}_{l,0} = c_l^x \vec{e}_x + c_l^y \vec{e}_y$ , and  $\vec{d}_l = \vec{D}_l - \vec{D}_{l,0} = d_l^x \vec{e}_x + d_l^y \vec{e}_y$ . Then, the Lagrange function in the harmonic approximation becomes  $L = T - V$  with

$$T = \frac{M}{2} \sum_{l=1}^L \left[ \left( \dot{a}_l^x \right)^2 + \left( \dot{b}_l^x \right)^2 + \left( \dot{c}_l^x \right)^2 + \left( \dot{d}_l^x \right)^2 \right],$$

$$V = \frac{K}{2} \sum_{l=1}^L \left[ (b_l^x - a_l^x)^2 + g (c_l^x - b_l^x)^2 + (d_l^x - c_l^x)^2 + [\cos(\phi) (a_{l+1}^x - d_l^x) - \sin(\phi) (a_{l+1}^y - d_l^y)]^2 \right]. \quad (\text{B4})$$

The variables  $b_l^y$  and  $c_l^y$  are cyclic and drop out of the problem.

## 2. Equations of motion

The Euler-Lagrange equations can be solved using the Fourier Ansatz

$$x_l(t) = e^{-i\omega t} \sum_{k=1}^L \xi_k e^{ikl} \quad (\text{B5})$$

with  $k = 2\pi m_k/L$ ,  $m_k = 0, 1, \dots, L-1$  as the crystal momentum. Here,  $\xi = (\alpha^x, \alpha^y, \beta^x, \gamma^x, \delta^x, \delta^y)$  corresponds to  $x = (a^x, a^y, b^x, c^x, d^x, d^y)$ . The resulting set of six algebraic equations can be cast into a matrix equation,  $\mathcal{M}(\omega) \vec{E}_k = (0, 0, 0, 0, 0, 0)^T$  for the vector  $\vec{E}_k = (\alpha_k^x, \alpha_k^y, \beta_k^x, \gamma_k^x, \delta_k^x, \delta_k^y)^T$ . With the abbreviations  $y = M\omega^2/K$ ,  $c = \cos(\phi)$ , and  $s = \sin(\phi)$ , the matrix reads

$$\mathcal{M}(\omega) = \begin{pmatrix} 1 + c^2 - y & -cs & -1 & 0 & -c^2 e^{-ik} & cse^{-ik} \\ -cs & s^2 - y & 0 & 0 & cse^{-ik} & -s^2 e^{-ik} \\ -1 & 0 & 1 + g - y & -g & 0 & 0 \\ 0 & 0 & -g & 1 + g - y & -1 & 0 \\ -c^2 e^{ik} & cse^{ik} & 0 & -1 & 1 + c^2 - y & -cs \\ cse^{ik} & -s^2 e^{ik} & 0 & 0 & -cs & s^2 - y \end{pmatrix}. \quad (\text{B6})$$

The equation for the vibrational frequencies  $\omega_n(k)$  as a function of the crystal momentum  $k$  results from the characteristic equation,  $\det(\mathcal{M}(\omega)) = 0$ .

We are interested in the optical phonon modes,  $\omega_n = \omega_n(k=0)$ . The characteristic equation reduces to

$$y^2(y-2)p(y) = 0, \quad (\text{B7})$$

$$p(y) = y^3 - 2(g+2)y^2 + (7/2 + 6g)y - 3g$$

for all  $g$  and  $\phi = 60^\circ$ . The finite-frequency solutions are denoted as  $\omega_n$  ( $n = a, b, c, d$ ). We set  $\omega_b = \sqrt{2K/M}$ , and  $\omega_a^2 < \omega_c^2 < \omega_d^2$  result from the three real roots of  $p(y) = 0$  in (B7) as  $\omega_{a,c,d} = \sqrt{Ky_{a,c,d}/M}$ .

## Appendix C: Bare dispersion relation

The operator for the kinetic energy  $\hat{T}$  in eq. (2) is readily diagonalized for periodic boundary conditions,  $N+1 \equiv 1$ . For the ground state of non-interacting electrons, the unit cell consists of four sites,  $N = 4L$ , and the electron transfer amplitudes follow the periodic pattern  $(t_s, t_t, t_s, t_d)$ . Thus, we may write

$$\hat{T} = - \sum_{\sigma} \sum_{n=0}^{L-1} \left( t_s \hat{c}_{4n+1,\sigma}^+ \hat{c}_{4n+2,\sigma} + t_t \hat{c}_{4n+2,\sigma}^+ \hat{c}_{4n+3,\sigma} + t_s \hat{c}_{4n+3,\sigma}^+ \hat{c}_{4n+4,\sigma} + t_d \hat{c}_{4n+4,\sigma}^+ \hat{c}_{4(n+1)+1,\sigma} \right) + \text{h.c.} \quad (\text{C1})$$

We introduce the four operators  $\hat{b}_{M;k,\sigma}$  for electrons with quasi-momentum  $k = -\pi + 2\pi m_k/L$ ,  $m_k = 0, 1, \dots, L-1$



via

$$\hat{b}_{M;k,\sigma} = \sqrt{\frac{1}{L}} \sum_{n=0}^{L-1} e^{-ikn} \hat{c}_{4n+M,\sigma} . \quad (\text{C2})$$

The inverse transformation reads

$$\hat{c}_{4n+M,\sigma} = \sqrt{\frac{1}{L}} \sum_k e^{ikn} \hat{b}_{M;k,\sigma} , \quad (\text{C3})$$

where we used that the sum over the quasi-momenta  $k$  generates the orthogonality relation

$$\frac{1}{L} \sum_k e^{ik(m-n)} = \delta_{m,n} \quad (\text{C4})$$

for two lattice indices  $m, n$ . In turn, the sum over lattice indices  $n$  leads to the orthogonality relation

$$\frac{1}{L} \sum_{n=0}^{L-1} e^{in(k-p)} = \delta_{k,p} \quad (\text{C5})$$

for two quasi-momenta  $k, p$ .

When we apply the transformation (C3) to the kinetic energy (C1), we obtain

$$\begin{aligned} \hat{T} = - \sum_{k,\sigma} & \left( t_s \hat{b}_{1;k,\sigma}^+ \hat{b}_{2;k,\sigma} + t_t \hat{b}_{2;k,\sigma}^+ \hat{b}_{3;k,\sigma} \right. \\ & \left. + t_s \hat{b}_{3;k,\sigma}^+ \hat{b}_{4;k,\sigma} + t_d e^{ik} \hat{b}_{4;k,\sigma}^+ \hat{b}_{1;k,\sigma} \right) + \text{h.c.} . \quad (\text{C6}) \end{aligned}$$

The remaining task is to band-diagonalize the kinetic energy. To this end we diagonalize the  $4 \times 4$ -matrix  $\mathcal{M}_k$  with

$$\mathcal{M}_k = \begin{pmatrix} 0 & -t_s & 0 & -t_d e^{-ik} \\ -t_s & 0 & -t_t & 0 \\ 0 & -t_t & 0 & -t_s \\ -t_d e^{ik} & 0 & -t_s & 0 \end{pmatrix} . \quad (\text{C7})$$

Its eigenvalues in ascending order are  $E_1(k) = -\epsilon_2(k)$ ,  $E_2(k) = -\epsilon_1(k)$ ,  $E_3(k) = \epsilon_1(k)$ ,  $E_4(k) = \epsilon_2(k)$  with

$\epsilon_1(k) < \epsilon_2(k)$ . We find<sup>17</sup>

$$\begin{aligned} [\epsilon_{1,2}(k)]^2 = & t_s^2 + t_d^2/2 + t_t^2/2 \\ & \pm \sqrt{(t_d^2 - t_t^2)^2/4 + t_s^2 [t_d^2 + t_t^2 + 2t_d t_t \cos(k)]} . \end{aligned} \quad (\text{C8})$$

We write

$$\mathcal{M}_k = \mathcal{U}_k^+ \mathcal{D}_k \mathcal{U}_k , \quad (\text{C9})$$

where  $\mathcal{D} = \text{diag}(-\epsilon_2(k), -\epsilon_1(k), \epsilon_1(k), \epsilon_2(k))$  is a diagonal matrix which contains the eigenvalues of  $\mathcal{M}_k$ . We define the band-diagonal operators

$$\begin{pmatrix} \hat{\alpha}_{k,\sigma} \\ \hat{\beta}_{k,\sigma} \\ \hat{\gamma}_{k,\sigma} \\ \hat{\delta}_{k,\sigma} \end{pmatrix} = \mathcal{U}_k \begin{pmatrix} \hat{b}_{1;k,\sigma} \\ \hat{b}_{2;k,\sigma} \\ \hat{b}_{3;k,\sigma} \\ \hat{b}_{4;k,\sigma} \end{pmatrix} \quad (\text{C10})$$

and find

$$\begin{aligned} \hat{T} = \sum_{k,\sigma} & \left[ \epsilon_2(k) \left( \hat{\delta}_{k,\sigma}^+ \hat{\delta}_{k,\sigma} - \hat{\alpha}_{k,\sigma}^+ \hat{\alpha}_{k,\sigma} \right) \right. \\ & \left. + \epsilon_1(k) \left( \hat{\gamma}_{k,\sigma}^+ \hat{\gamma}_{k,\sigma} - \hat{\beta}_{k,\sigma}^+ \hat{\beta}_{k,\sigma} \right) \right] . \quad (\text{C11}) \end{aligned}$$

The  $\alpha$ - and  $\beta$ -bands are the valence bands which are filled in the ground state at half band-filling. The  $\gamma$ - and  $\delta$ -bands are the conduction bands which are empty in the half-filled ground state.

The bare gap at half band-filling obeys  $\Delta^{\text{bare}} = 2\epsilon_1(0)$  with

$$[\epsilon_1(0)]^2 = t_s^2 + t_d^2/2 + t_t^2/2 - \sqrt{4t_s^2 + (t_t - t_d)^2} (t_d + t_t)/2 . \quad (\text{C12})$$

For small deviations,  $t_s, t_d, t_t \approx t_0$ , this simplifies to<sup>17</sup>

$$\Delta^{\text{bare}} \approx |t_t + t_d - 2t_s| . \quad (\text{C13})$$

<sup>1</sup> *Polydiacetylenes*, ed. by H.-J. Cantow (Advances in Polymer Sciences **63**, Springer, Heidelberg, 1984); *Polydiacetylenes*, ed. by D. Bloor and R.R. Chance (Nijhoff, Dordrecht, 1985).

<sup>2</sup> *Primary photoexcitations in conjugated polymers*, ed. by N.S. Sariciftci (World Scientific, Singapore, 1997).

<sup>3</sup> M. Schott, in *Photophysics of molecular materials: from single molecules to single crystals*, ed. by G. Lanzani (Wiley-VCH, Weinheim, 2006), p. 49.

<sup>4</sup> S. Spagnoli, J. Berrkhar, C. Lapersonne-Meyer, and M. Schott, *J. Chem. Phys.* **100**, 6195 (1994).

<sup>5</sup> F. Dubin, R. Melet, T. Barisien, R. Grousson, L. Legrand, M. Schott, and V. Voliotist, *Nature Physics* **2**, 32 (2006).

<sup>6</sup> D.E. Parry, *Chem. Phys. Lett.* **43**, 597 (1976); *Chem. Phys. Lett.* **46**, 605 (1977).

<sup>7</sup> S. Yang and M. Kertesz, *J. Phys. Chem. A* **110**, 9771 (2006).

<sup>8</sup> B.G. Janesko, *J. Chem. Phys.* **134**, 184105 (2011).

<sup>9</sup> B.G. Janesko, private communication (2011).

<sup>10</sup> M. Rohlfing and S.G. Louie, *Phys. Rev. Lett.* **82**, 1959 (1999).

<sup>11</sup> J.-W. van der Horst, P.A. Bobbert, M.A.J. Michels, G. Brocks, and P.J. Kelly, *Phys. Rev. Lett.* **83**, 4413 (1999); J.-W. van der Horst, P.A. Bobbert, P.H.L. de Jong, M.A.J. Michels, G. Brocks, and P.J. Kelly, *Phys. Rev. B* **61**, 15817 (2000); J.-W. van der Horst, P.A. Bobbert, and M.A.J.

- Michels, Phys. Rev. B **66**, 035206 (2002).
- <sup>12</sup> J.-W. van der Horst, P.A. Bobbert, M.A.J. Michels, and H. Bäßler, J. Chem. Phys. **114**, 6950 (2001).
- <sup>13</sup> A. Grage, F. Gebhard, and J. Rissler, J. Stat. Mech. Exp. Theor. P08009 (2005).
- <sup>14</sup> R. Pariser and R.G. Parr, J. Chem. Phys. **21**, 466 (1953); J.A. Pople, Trans. Farad. Soc. **49**, 1375 (1953).
- <sup>15</sup> S.R. White, Phys. Rev. Lett. **69**, 2863 (1992); Phys. Rev. B **48**, 10345 (1993).
- <sup>16</sup> G. Barcza, Ö. Legeza, F. Gebhard, and R.M. Noack, Phys. Rev. B **81**, 045103 (2010).
- <sup>17</sup> A. Race, W. Barford, and R.J. Bursill, Phys. Rev. B **64**, 035208 (2001).
- <sup>18</sup> A. Race, W. Barford, and R.J. Bursill, Phys. Rev. B **67**, 245202 (2003).
- <sup>19</sup> K. Ohno, Theor. Chim. Acta **2**, 219 (1964).
- <sup>20</sup> M. Chandross, S. Mazumdar, M. Liess, P.A. Lane, Z.V. Vardeny, M. Hamaguchi, and K. Yoshino, Phys. Rev. B **55**, 1486 (1997); M. Chandross and S. Mazumdar, Phys. Rev. B **55**, 1497 (1997).
- <sup>21</sup> T.D. Kobelt and E.F. Paulus, Acta Crystallogr. B **30**, 232 (1974).
- <sup>22</sup> For a review, see M. Schott and G. Wegener, in *Nonlinear Optical Properties of Organic Molecules and Crystals*, Vol. 2, ed. by D.S. Chemla and J. Zyss (Academic Press Inc., London, 1987), p. 3.
- <sup>23</sup> S. Spagnoli, J. Berrehar, J.-L. Fave, and M. Schott, Chem. Phys. **333**, 254 (2007).
- <sup>24</sup> A. Horvath, G. Weiser, C. Lapersonne-Meyer, M. Schott, and S. Spagnoli, Phys. Rev. B **53**, 13507 (1996).
- <sup>25</sup> G. Weiser, private communication (2012).
- <sup>26</sup> R. Loudon, Am. J. Phys. **27**, 649 (1959).
- <sup>27</sup> L. Bányai, I. Galbraith, C. Ell, and H. Haug, Phys. Rev. B **36**, 6099 (1987).
- <sup>28</sup> A.J. Heeger, S. Kivelson, J.R. Schrieffer, and W.-P. Su, Rev. Mod. Phys. **60**, 781 (1988).
- <sup>29</sup> E. Ehrenfreund, Z. Vardeny, O. Brafman, and B. Horovitz, Phys. Rev. B **36**, 1535 (1987).
- <sup>30</sup> See, for example, J. Sólyom, *Fundamentals of the Physics of Solids*, Vol. 3 (Springer, Berlin, 2010), chap. 30.
- <sup>31</sup> G. Weiser, Phys. Rev. B **45**, 14076 (1992).
- <sup>32</sup> Ö. Legeza, J. Röder, and B.A. Hess, Phys. Rev. B **67**, 125114 (2003).
- <sup>33</sup> Ö. Legeza and J. Sólyom, Phys. Rev. B **70**, 205118 (2004).
- <sup>34</sup> G. Barcza, Ö. Legeza, K.H. Marti, and M. Reiher, Phys. Rev. A **83**, 012508 (2011).
- <sup>35</sup> G.B.B.M. Sutherland and D.M. Dennison, Proc. Roy. Soc. A **148**, 250 (1935).
- <sup>36</sup> A.V. Jones, Proc. Roy. Soc. A **211**, 285 (1952).
- <sup>37</sup> A. Girlando, A. Painelli, G.W. Hayden, and Z.G. Soos, Chem. Phys. **184**, 139 (1994).
- <sup>38</sup> G. Herzberg, *Infrared and Raman Spectroscopy of polyatomic molecules* (van Nostrand, New York, 1945).
- <sup>39</sup> C.S. Yannoni and T.C. Clarke, Phys. Rev. Lett. **51**, 1191 (1983).
- <sup>40</sup> G. Barcza, PhD thesis (Budapest, 2013, unpublished).
- <sup>41</sup> S. Mazumdar, Z. Wang, and H. Zhao, in *Ultrafast Dynamics and Laser Action of Organic Semiconductors*, ed. by Z.V. Vardeny (CRC Press, Boca Raton, USA, 2009), p. 77.
- <sup>42</sup> J. Rissler, H. Bäßler, F. Gebhard, and P. Schwerdtfeger, Phys. Rev. B **64**, 045122 (2001); J. Rissler, F. Gebhard, and E. Jeckelmann, J. Phys. Cond. Matt. **17**, 4093 (2003).